The effect of a hydraulic parameterisation of overflows on the ocean circulation

Andreas Born

21. Dezember 2006

Diplomarbeit im Fach Physik

eingereicht an der
Mathematisch–Naturwissenschaftliche Fakultät
Universität Potsdam

Gutachter:

Prof. Dr. Anders Levermann
Institut für Physik, Universität Potsdam
Potsdam Institut für Klimafolgenforschung

Prof. Dr. Stefan Rahmstorf
Institut für Physik, Universität Potsdam
Potsdam Institut für Klimafolgenforschung

C & A

Abstract

The aim of this study is to investigate the sensitivity of a coarse resolution fully coupled climate model to the representation of the overflows over the Greenland–Scotland Ridge. This class of models suffer from a poor representation of the water mass exchange between the Nordic Seas and the North Atlantic, a crucial part of the Atlantic meridional overturning circulation (AMOC). We revise the explicit representation of the overflows by a parameterisation by hydraulic constraints and compare it with the enhancement of the overflow transport by artificially deepened passages over the Greenland–Scotland Ridge, a common practice in coarse resolution models.

Special attention will be paid to changes in the subpolar gyre circulation. We find it sensitive to the overflow transport and the density of these water masses through the joint effect of baroclinicity and relief (JEBAR). The analysis of the governing equations isolates the influence of the overflows on the dynamics of the subpolar gyre. On the basis of this understanding we construct three positive feedback loops that control the subpolar gyre and allow for bistability.

Einfluß einer hydraulischen Parametrisierung der Überströmung von Schwellen auf die Ozeanzirkulation

Zusammenfassung

Diese Arbeit behandelt die Empfindlichkeit eines grob aufgelösten, vollständig gekoppelten Klimamodells von der Darstellung der Überströmung des unterseeischen Rückens zwischen Grönland und Schottland. Bei dieser Art von Modellen ist die Simulation des Wassermassenaustausches zwischen dem Nordmeer und dem Nord Atlantik besonders schwierig. Dabei handelt es sich um einen wichtigen Teil der atlantischen meridionalen Umwälzzirkulation (AMOC). Die Implementierung einer Parametrisierung der Überströmprozesse wird verglichen werden mit der Steigerung des Transportes durch die künstliche Absenkung der tiefen Passagen des unterseeischen Rückens. Letzteres ist ein verbreitetes Vefahren bei grob aufgelösten Ozeanmodellen.

Besondere Beachtung wird die Zirkulation des subpolaren Wirbels erhalten. Es stellt sich heraus, dass sie empfindlich von den überströmenden Wassermassen abhängt und dass der Grund dafür im so genannten JEBAR Effekt liegt. Die Analyse der zugrundeliegenden Bewegungsgleichungen zeigt den Einfluß der überströmenden Wassermassen auf den subpolaren Wirbel auf. Mit Hilfe dieses Veständnisses können drei verstärkende Rückkopplungsmechanismen identifiziert werden, die den subpolaren Wirbel steuern und eine Bistabilität ermöglichen.

Contents

1 Introduction

The submarine ridges between Greenland and Scotland (GSR) play a key role in the formation of North Atlantic Deep Water (NADW) (Dickson and Brown, 1994; Hansen and Østerhus, 2000; Hansen et al., 2004). Exchange between the Atlantic and the deep water formation sites in the Nordic Seas is limited by this barrier. The overflows of dense deep water from the Nordic Seas over the ridge form fast, buoyancy driven bottom currents. As they flow over the GSR, the overflows mix with the surrounding warmer North Atlantic waters to become NADW (Hansen and Østerhus, 2000). Thus, the overflows play an important role in the Atlantic meridional overturning circulation (AMOC) (Kuhlbrodt et al., 2006; Redler and Böning, 1997). The potential energy stored in the dense water reservoir in the Nordic Seas may have a stabilising effect on the AMOC (Lohmann, 1998) which is of great interest in the framework of climate change. A shutdown of the overflow transport and the successive reorganisation of the AMOC would weaken the heat transport to the high northern latitudes and rise sea levels by several decimeters in the North Atlantic (Levermann et al., 2005). Although the process of deep water formation in the Nordic Seas is highly seasonal because it depends on the strong winter cooling on the surface, the overflow transport does not show this seasonality. Available direct observations of Nordic seas overflows do not show significant trend in the last decade (Hansen and Østerhus, 2000).

One characteristic of the overflows is the narrow passages by which they are formed. This causes their problematic representation particulary in coarse resolution models. In order to simulate the overflow transport, these models typically use artificially deepened and broadened passages (Roberts and Wood, 1997; Thorpe et al., 2004). Here, we will reassess this aproach and compare it to a parameterisation by hydraulic constrains following Kösters (2004) which was first implemented into a coarse resolution ocean model by Kösters et al. (2005). This parameterisation allows the use of the realistic topography.

The presented study will be organised as follows. We start with an overview of the general oceanic circulation of the Atlantic Ocean where we focus on the characteristics we discuss in successive sections. Subsequently, we review the water mass exchanges between the Nordic Seas and the North Atlantic more in detail.

After a short description of our climate model CLIM*BER*-3α and some technical details of the hydraulic overflow parameterisation, we compare the parameterised model version with the current standard version. First, we present phenomenological differences between the two equilibrium climate states and then proceed to track the physical mechanisms underlying the observed changes. The identification of these mechanisms allows not only to estimate the influence of the overflows and a possible parameterisation of their volume transport on the Atlantic subpolar region but also completes a set of recently reported feedbacks in the subpolar gyre circulation in the way that a bistability of the entire system is found. To conclude we analyse the stability of the overflow parameterisation to anomalous freshwater flux into the subtropical Atlantic Ocean.

2 The circulation in the Atlantic Ocean

The circulation of the Earth's fluids, oceanic and atmospheric, is determined by a variety of factors. Surface fluxes of heat, freshwater and momentum, as well as gravity, tides and the Earth's rotation set the ocean waters in motion, either directly or via intermediate processes such as waves (Kuhlbrodt et al., 2006). Geothermal processes affect the circulation near the mid–oceanic ridges or similar tectonically active regions but only on small spatial scales.

Deep ocean currents are driven by density gradients, that is by variations in the temperature and salinity distribution. The thermohaline circulation, also known as the ocean's conveyor belt, refers to a deep ocean current system covering the entire world ocean (Fig. 1).

2.1 Horizontal circulation, gyres

Surface ocean currents are generally wind driven and develop clockwise gyres in the northern hemisphere and counter-clockwise rotation in the southern hemisphere because of the imposed wind stresses. They span from coast to coast in the subtropical oceans and form strong and narrow western boundary currents. In the Atlantic, this current is the Gulf Stream in the northern hemisphere and the Brazil Current for the southern subtropical gyre system. Western boundary currents are essential to

assure vorticity conservation in the ocean.

North of the northern hemisphere subtropical gyre in the Atlantic, a cyclonic gyre spins, the subpolar gyre. On its eastern side, warm, saline subtropical waters from the Gulf Stream extension enter the gyre from the south while in the northwest the East Greenland Current brings cold and relatively fresh water masses from Artic origin. The balance of the resulting density contrast is found to have a profound influence on the subpolar gyre strength as opposed to the subtropical gyres, which are believed to be essentially wind driven (Greatbatch et al., 1991; Myers et al., 1996; Penduff et al., 2000; Eden and Willebrand, 2001).

2.2 Atlantic meridional overturning circulation

Superimposed to these superficial gyres there is another circulation that includes the deep ocean, the Atlantic meridional overturning circulation (AMOC) (Fig. 1). The AMOC is an interhemispheric circulation that influences climate regionally as well as globally (Vellinga and Wood, 2002; Levermann et al., 2005; Timmermann et al., 2005; Schmittner, 2005). In the North Atlantic, its maximum northwards heat transport is about 1 PW (10^{15} W) (Hall and Bryden, 1982; Ganachaud and Wunsch, 2000; Trenberth and Caron, 2001). The AMOC consists of four branches: upwelling processes that transport volume from depth near the ocean surface, surface currents that transport relatively light water towards high northern latitudes, deep water formation regions where waters become denser and sink, and deep currents closing the loop. These four branches span the entire Atlantic on both hemispheres, forming a circulation system that consists of two overturning cells, a deep one with North Atlantic Deep Water (NADW) and an abyssal one with Antarctic Bottom Water (AABW) (Kuhlbrodt et al., 2006). On the southern side the AMOC is connected to a global circulation system by the Antarctic Circumpolar Current (ACC) (Fig. 1). However, the other ocean basins do not show a meridional overturning circulation with northern sinking. In the Pacific Ocean no deep convection occurs and its surface waters are fresher than in the Atlantic.

For climate on multi–decadal to millenial time–scales, the AMOC plays a crucial role as it connects the deep ocean to the surface. The deep ocean can store vast amounts of heat and chemical species such as carbon dioxide. The strength of its

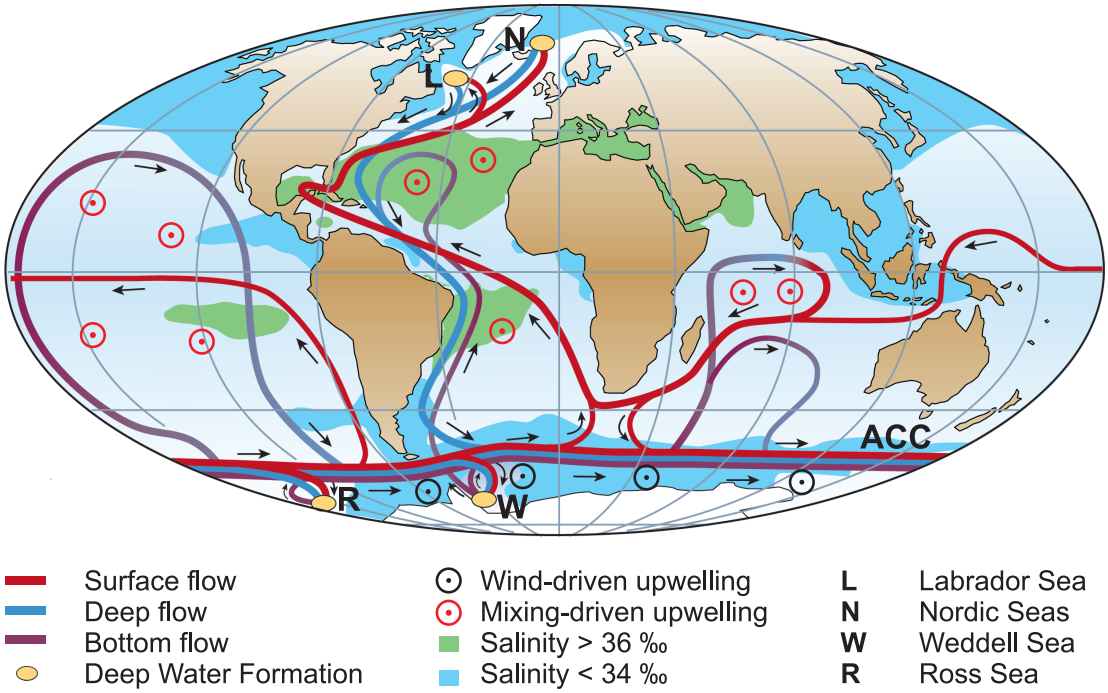

Figure 1: Simplified sketch of the meridional overturning circulation system. The atlantic branch is referred to as the Atlantic meridional overturning circulation (AMOC). It consists of a warm and saline surface current that flows northwards, cools in the high northern latitudes and sinks in the Labrador and Nordic Seas. After sinking it returns at depth. By contrast, there is no deep water formation in the Pacific and its surface waters are fresher. Deep water formation also occurs in the Southern Ocean. These waters are denser and hence spread over deeper levels than those from the North Atlantic. In contrast to the localised downwelling, upwelling occurs wide spread by two processes, mixing–driven and wind–driven in the Southern Ocean due to the Drake Passage effect (Kuhlbrodt et al., 2006).

ventilation hence determines the inertial effect of the ocean in the climate system and influences transient changes. Further, the AMOC affects the climate system due to the interhemispheric heat transport.

Presently, two distinct mechanisms for driving the AMOC are discussed. The first one is the thermohaline driving mechanism (Munk and Wunsch, 1998). In this view, turbulent mixing of heat lightens water masses in the deep ocean and causes them to rise in low latitudes. This turbulent mixing is mainly due to small–scale motions induced by the breaking of internal waves generated by winds and tides (Kuhlbrodt et al., 2006). Recently, evidence emerged that significant mixing can also be caused by migrating krill, a small shrimplike species, particulary in nutrient–rich southern ocean waters (Kunze et al., 2006). The resulting surface waters are then advected northwards into the North Atlantic, where they are transformed into dense waters by atmospheric cooling and salt rejection during sea-ice growth. These waters sink to depth, setting up the deep water mass of the ocean. Thereby a meridional density gradient between high and low latitudes is established in the deep ocean, which leads to a deep southwards return flow (Griesel and Maqueda, 2006).

The second mechanism is wind-driven upwelling, proposed by Toggweiler and Samuels (1993, 1995, 1998). Based on observational radiocarbon constraints, they concluded that the actual amount of upwelling of abyssal water caused by diapycnal mixing is insufficient to sustain an estimated overturning of about 15 Sv (1 Sv = 1 Sverdrup = $10^6 m^3 s^{-1}$) in the Atlantic Ocean. As an alternative, they suggested that most of the oceanic upwelling is wind-driven and occurs in the Southern Ocean due to the so-called Drake Passage effect. The latitude band of the Drake Passage is the only region on Earth without meridional topographic boundaries (except for the Arctic Ocean). Hence no zonal density gradient can establish and no net geostrophic volume transport in meridional direction balances the wind–driven transport at this latitude. Strong westerly circumpolar winds induce a northwards transport of waters, called Ekman transport, near the ocean surface. This unbalanced horizontal divergence of the Ekman transports can only be compensated by an large–scale upwelling from depth, which must not be mistaken for a mixing process by small–scale turbulence induced by wind. In this view, it is the strength of Southern Ocean winds rather than the oceanic diapycnal mixing that governs the strength of the AMOC.

Determining which of these two processes is the main driving mechanism of the AMOC is of great interest, even beyond the aim of physical understanding. The two could imply different sensitivities to variations in external forcing (Schmittner and Weaver, 2001; Prange et al., 2003), and thus different evolution of the AMOC under continued global climate change. For a comprehensive discussion of both processes, as well as a review on the theory, modelling experience and observations, please refer to Kuhlbrodt et al. (2006).

Both proposed mechanisms for the driving of the AMOC are upwelling processes, as in this one of the four branches energy input is needed not only to balance friction. The sinking processes in the high latitudes play an important role also, but rather for the shape of the AMOC than its maximum strength (Kuhlbrodt et al., 2006). This implies, however, that Nordic Seas deep water formation locally does determine the strength of the meridional overturning over the GSR and inside the Nordic Seas. In addition, the rate and region of deep water formation prescribes the vertical density gradient throughout the entire Atlantic ocean and may thus be of second order importance, at least if vertical mixing is important as a driving mechanism.

In a simplified view, the strength of the overturning circulation in the North Atlantic depends on the amount of saline water transported to the deep water formation regions. As this amount depends on the strength of the meridional circulation again, the AMOC is part of a positive feedback loop. This auto–amplification by the so–called salt feedback gives the AMOC a nonlinear response upon freshwater forcing and two stable circulation modes, with and witout NADW formation (Stommel, 1961; Rahmstorf, 1996). A number of ocean models confirm this behaviour (Manabe and Stouffer, 1988; Rahmstorf et al., 2005). Reorganisations of the AMOC have been suggested as explanation for a various paleoclimatic events (see reviews by Clark et al. (2002); Rahmstorf (2002)) (Bauer et al., 2004).

3 The North Atlantic – Nordic Seas exchanges

The water mass exchange between the North Atlantic and the Nordic Seas is probably the best–investigated process in the global ocean. This special interest arises from the fact that the Nordic Seas represent one of the oceanic deep convection re-

gion in the northern hemisphere. Hence the Greenland–Scotland ridge (GSR) plays a key role as it separates the North Atlantic in the south from the Nordic seas in the north. This separation is not complete, the remaining passages are broader and deeper than the Bering Strait that divides the Pacific Ocean from the Arctic. Yet the GSR represents a severe obstacle to crossing ocean currents. In recent decades a wealth of studies has been published concerning the exchange over the GSR, the topography of the submarine ridges and the pathways of the deep currents (Dickson and Brown, 1994; Hansen and Østerhus, 2000; Østerhus et al., 2005; Kieke and Rhein, 2006). We will rely on the one of Hansen and Østerhus (2000), which also is the most comprehensive to date.

3.1 Bottom topography of the Greenland–Scotland ridge

The GSR extends from East Greenland to Scotland and forms a continuous barrier below 840 m. It is divided into three main gateways by Iceland and the Faroe Islands, each one with different characteristics (Fig. 2). From northwest to southeast the first gap is the Denmark Strait, which has a maximum depth of about 620 m and is relatively wide. To the east of Iceland follows an even wider part but also very shallow, deepening towards the Faroese side to a maximum of 480 m. The deepest passage of the GSR is part of a more complex topography on the eastern and southern side of the Faroe Islands. Between the Faroes and the Scottish shelf, the broad and deep Faroe–Shetland Channel intersects the GSR but is blocked by the Wyville–Thomson Ridge with sill depth around 600 m on the southern end. It discharges into the narrow Faroe Bank Channel with sill depth around 840 m (Hansen and Østerhus, 2000). To the north of the GSR the Nordic Seas extend, i.e. the Iceland Sea, the Norwegian Sea, the Greenland Sea and the fairly shallow Barents Sea (see Fig. 3). As the Nordic Seas are not part of the Arctic Ocean, but share certain characteristics with it, the term ‘Arctic Mediterranean’ has been introduced that comprises both. The adjacent region of the North Atlantic on the southern side of the GSR is divided by the Mid–Atlantic Radge into two deep basins, the Irminger Basin and the Iceland Basin (Fig. 3).

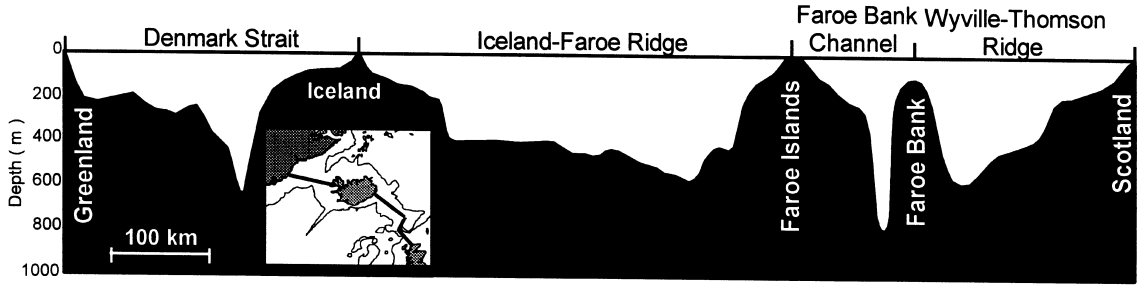

Figure 2: Bottom depth along the oceanic part of a section following the crest of the Greenland–Scotland Ridge (shown on the inset map) (Hansen and Østerhus (2000, fig. 2))

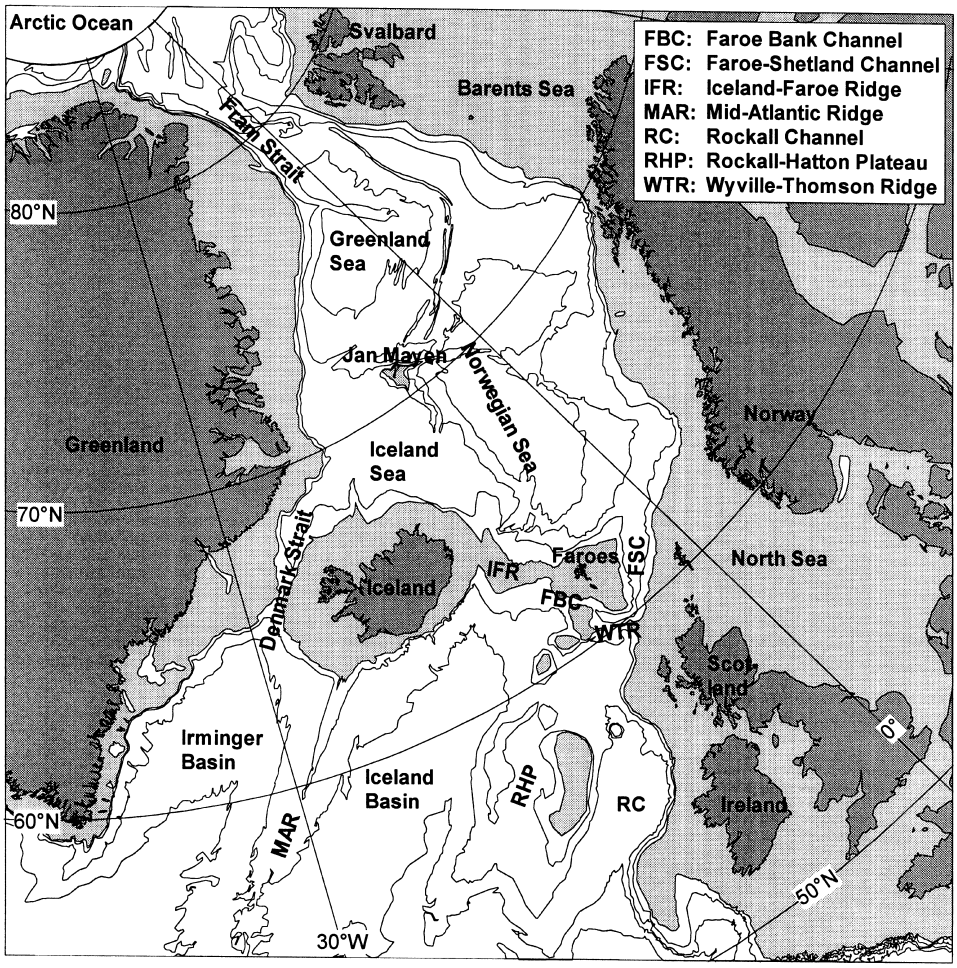

Figure 3: Topography of the GSR and surrounding regions. Areas shallower than 500 m are lightly shaded (Hansen and Østerhus, 2000, fig. 1).

3.2 Exchange paths

Flow over the GSR is characterised by a near surface inflow, the Atlantic inflow, and a deep outflow at depth over the previously portrayed passages, commonly referred to as overflow. The major flows in the surface are shown in figure 4. The Atlantic inflow has several branches, the most prominent being the North Atlantic Current, part of which passes the GSR west of Iceland through the Denmark Strait (the North Icelandic Irminger Current). However, the biggest fraction flows across the eastern side of the GSR (Faroe Current and Shetland Current). In addition to these three 'oceanic' branches, there is also a persistent flow of Atlantic water northeastwards over the continental slope, termed the Continental Slope Current (Hansen and Østerhus, 2000). Hátún et al. (2005) showed that on interannual to interdecadal time scales, the salinity of the Atlantic inflow to the Arctic Mediterranean depends mainly on the relative contributions of the these two currents that are controlled by the dynamics of the subpolar gyre circulation. Although we stated before that surface currents enter the Nordic Seas, this is not true for the East Greenland Current. It exports cold and fresh artic water along the slope of Greenland into the North Atlantic, where it further follows the coast into the Labrador Sea. But while the other currents across the GSR share the same forcing processes, as will become clear in the next section, the East Greenland Current is not an essential part of this system and will therefore not be discussed in detail in this work. Neither will the precise flow paths or origins of the other introduced currents, as the resolution of our ocean model would not permit any accurate conclusion in this point.

The flow paths at depth are constrained by the topography. Hence there exist three main gateways, the Denmark Strait, the Iceland–Faroe Channel and the Faroe Bank Channel. After passing the ridges, the overflow water, along with entrained Atlantic water, flows as density driven bottom current into the adjacent basins. The water from the eastern passages passes the Mid–Atlantic Ridge further south to join the Denmark Strait overflow water. Virtually the entire overflow waters combine to flow westward past Cape Farewell on the southern tip of Greenland (Dickson and Brown, 1994) (see fig. 5, right). Hansen and Østerhus (2000) give a water balance of the Arctic Mediterranean including the transports across the Bering Strait and the Canadian Archipelago, here shown in figure 5 (left). Note also the more comprehensive view from Dickson and Brown (1994) (fig. 5, right)

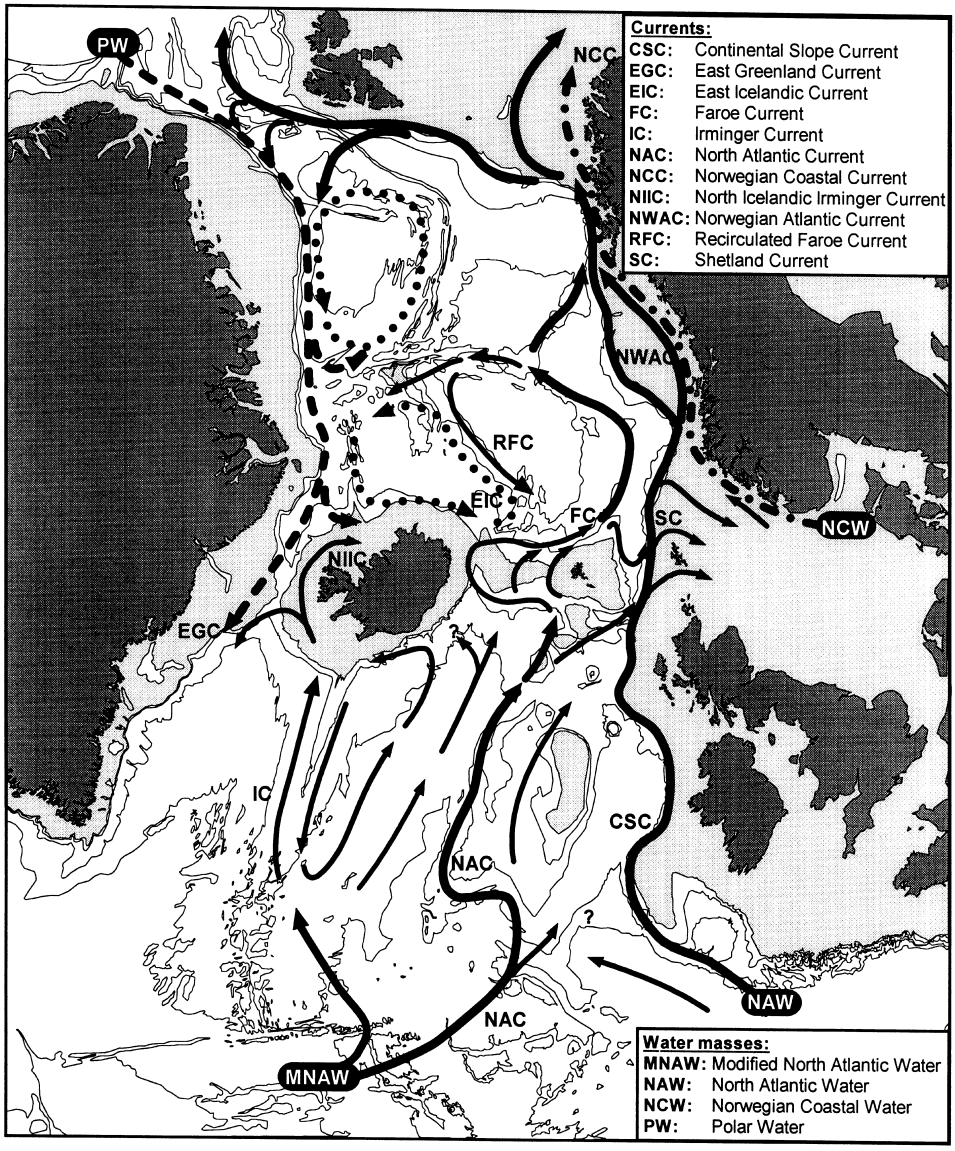

Figure 4: Main features of the near surface circulation in the eastern North Atlantic and the Nordic Seas. Continuous arrows show Atlantic water flow, broken and dotted arrows indicate flow of other water masses. The Atlantic inflow into the Nordic Seas ocurrs mainly on the eastern side of the GSR. Its composition is determined by the mixing ratio of North Atlantic water and North Atlantic water that was modified by the subpolar gyre circulation (from Hansen and Østerhus (2000, fig. 5)).

with a higher spatial accuracy and estimates for entrainment. It is based on various mesurements with current meter arrays.

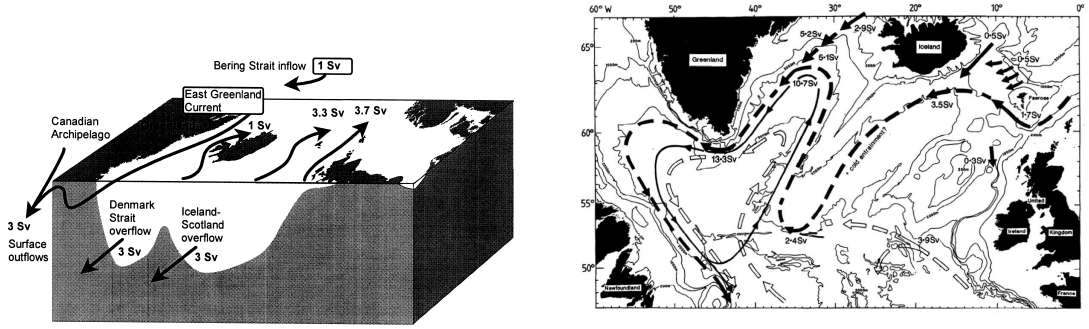

Figure 5: Sketch of the water exchange over the GSR as proposed by Hansen and Østerhus (2000) (left). Dickson and Brown (1994) (right) give an overview of the dense water overflows based on a variety of measuments. Dickson and Brown (1994) also show the flow paths of the NADW.

3.3 Forcing

The dominant effect for across GSR transport is due to pressure gradients established by thermohaline processes in the Arctic Mediterranean (e.g. deep convection). Other driving mechanisms like wind stress or estuarine forcing have only small effect on the mass exchange but affect the properties of the inflowing water and its distribution within the Arctic Mediterranean (Hansen and Østerhus, 2000). Convection sets up horizontal density and pressure gradients inside the Nordic Seas that drive the overflows. These in turn induce a pressure gradient in the surface which is compensated by the Atlantic inflow. If not, the uncompensated overflow of 6Sv would lower the surface of the Arctic Mediterranean by more than one meter a month (Hansen and Østerhus, 2000). In the balance presented in figure 5, two thirds of the inflowing water are returned in the deep overflows. In other words, most of the inflowing water transforms to deep water and returns at depth following the AMOC loop.

4 Description of the model CLIM*BER*-3α and experimental set–up

The model used in this study is the CLIM*BER*-3α coupled climate model of intermediate complexity (Montoya et al., 2005). It consists of the statistical–dynamical atmospheric model POTSDAM-2 (Petoukhov et al., 2000) coupled to a global, 24-layer ocean general circulation model based on the Geophysical Fluid Dynamics Laboratory (GFDL) Modular Ocean Model (MOM-3) code and to the dynamic and thermodynamic sea ice module of Fichefet and Maqueda (1997). The oceanic horizontal resolution is $3.75° \times 3.75°$. We apply a weak background vertical diffusivity of $0.2 \times 10^{-4} \frac{cm^2}{s}$. For a discussion on the model's sensitivity to oceanic vertical diffusivity refer to Mignot et al. (2006). A second–order moment tracer advection scheme is implemented (Prather, 1986), which minimises numerical diffusivity (Hofmann and Maqueda, 2006), and a parameterisation of boundary enhanced mixing depending both on near–bottom stratification and roughness of topography (Ledwell et al., 2000), following Hasumi and Suginohara (1999). This leads locally to vertical diffusion coeffcients of up to $10^{-4} \frac{cm^2}{s}$ over rough topography for example.

The atmospheric submodel has a coarse spatial resolution (7.5° in latitude and 22.5° in longitude) and is based on the assumption of a universal vertical structure of temperature and humidity, which allows reducing the three-dimensional description to a set of two-dimensional prognostic equations for temperature and humidity. Description of atmospheric dynamics is based on a quasi-geostrophic approach and a parameterisation of the zonally averaged meridional atmospheric circulation. The synoptic processes are parameterised as diffusion terms with a turbulent diffusivity computed from atmospheric stability and horizontal temperature gradients. Heat and freshwater fluxes between the ocean and the atmosphere are computed on the oceanic grid and applied without any flux adjustments. The wind stress is computed as the sum of the NCEP-NCAR reanalysis wind stress climatology (Kalnay and Coauthors, 1996) and the wind stress anomaly calculated by the atmospheric model relative to the control run.

For the present work we carried out three different series of experiments. The first one models the overflows with an artificially deepened topography (DEEP). This is the standard set–up of the model as described in Montoya et al. (2005) irrespective of

a higher background vertical diffusivity. The second experiment differs from DEEP in that the sills of the GSR region have their realistic depth (CTRL) and the third combines the same realistic topography with the hydraulic overflow parametrisation (HYDRO) (Fig. 8). Additional experiments are introduced when needed, but we will refer to the three presented here throughout the entire work. Unless declared otherwise, the results presented are multidecadal averages of experiments run into equilibrium for at least 2000 years.

5 Description of the hydraulic overflow parameterisation

The flow through narrow passages in coarse resolution models is a long lasting problem in ocean modelling. It is common practice to deepen and broaden the pathways artificially in order to achieve a realistic volume transport. Recently, hydraulic constraints were proposed to parameterise the overflow transport in these models, based on theoretical work done by Whitehead et al. (1974), and successfully implemented in a global ocean GCM (Kösters et al., 2005). This parameterisation allows the use of the realistic topography. The overflow transport is calculated by the large scale tracer distribution as

$$Q_{max} = \frac{g}{f\rho_0} \int_h^\eta (\rho_N(z) - \rho_S(z)) z dz, \tag{1}$$

where Q is the maximum hydraulic overflow transport, computed by an integral from the sill level h to the surface η. ρ_N, ρ_S and ρ_0 are the horizontally averaged but depth dependent densities north and south of the GSR and the mean density, z the local depth and g and f the gravitational constant and the coriolis parameter. Note that the integral can be interpreted as the potential energy difference of the water masses above sill level between two regions north and south of the GSR.

Please also note the comments we make on equation (1) in appendix B.

We choose the regions to cover the whole Nordic seas from the Greenland coast to 20°E and the entire North Atlantic in the latitude band between 45°N and the GSR at 63°N (Fig. 7). The GSR passages were corrected to more realistic sill depths

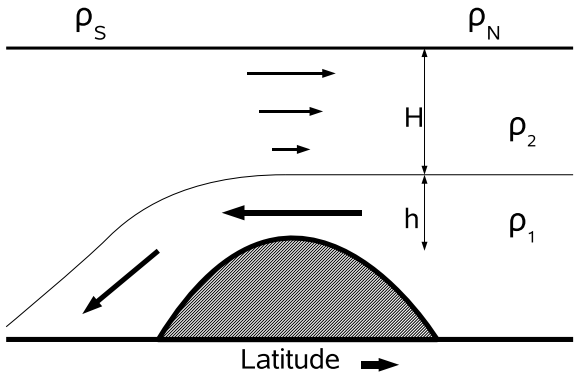

Figure 6: Sketch of the overflow region. A northwards surface flow balances the southwards overflow at depth and brings warm and saline water masses to high latitudes. The maximum overflow transport Q_{max} is calculated from the difference of the horizontally averaged potential energy north and south of the GSR (eq. (1)).

and shapes (Fig. 8).

6 Performance of the hydraulic overflow parameterisation

The comparison of the two unparameterised model version, DEEP and CTRL, reveals major differences in the Atlantic meridional overturning circulation (AMOC) (Fig. 9). With realistic topography the circulation in the Nordic Seas stops and the AMOC is generally weaker. The Nordic Seas deep convection is weaker and further south in CTRL, as can be inferred from the shallower mixed layer depth (Fig. 10). Due to the coarse resolution, Labrador Sea deep convection is shifted to the east into the Irminger Sea. Over the artificially deepened passages in DEEP overflows can pass the ridge in southward direction and surface currents flow northwards in order to compensate the outflow (Fig. 8). The presence of water of tropical origin allows deep convection and a circulation in the Nordic Seas (Fig. 9 and 10). In CTRL, the Nordic Seas are virtually disconnected from the North Atlantic, the GSR overflows do not exist here.

In HYDRO deep convection occurs in roughly the same areas as in DEEP, mainly north of the GSR and partly in the Irminger Sea (Fig. 10). The mixed layer

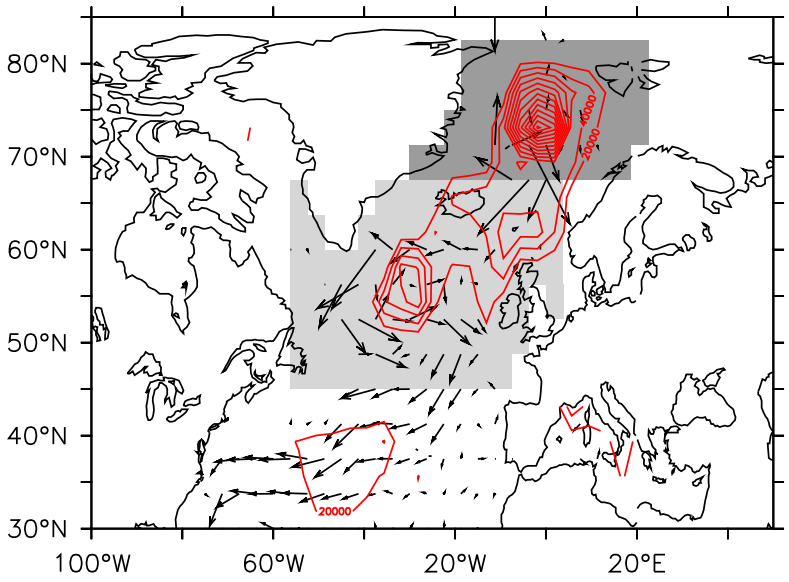

Figure 7: Control regions in the North Atlantic and Nordic Seas (grey). The maximum overflow transport across the GSR as calculated from equation (1) is proportional to the difference in potential energy above sill level in these regions. Contours are the mixed layer depth of one of the dicussed experiments, vectors the transport below 1000 m, both for orientation only.

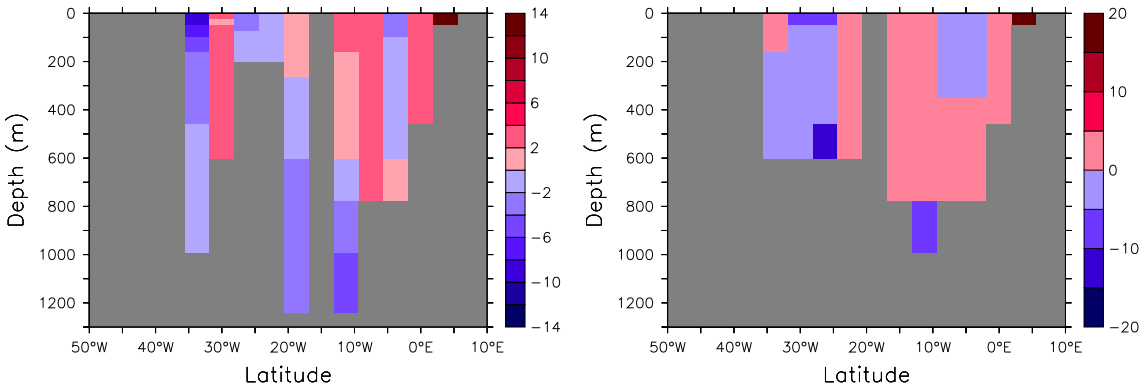

Figure 8: Section along the Greenland–Scotland Ridge through Iceland. Colours: Meridional velocity component, negative means southwards (cm/s) Right: Topography of experiment DEEP with artificially deepened passages and shifted Iceland. The deep overflow transport ocurrs mainly through the deep passages. Left: Topography of the experiments HYDRO and CTRL with more realistic sill depths for the Denmark Strait and the Faroe–Shetland Channel. The parameterised overflows are identified by the two grid cells with strong southwards velocities.

	AMOC max.	Overflow	SOO	NADW depth [m]	SPG
DEEP	13.16	7.29	10.34	2700	18.4
HYDRO	12.55	3.92	9.65	2500	28.3
CTRL	10.92	2.48	6.94	2200	10.1

Table 1: Properties of the Atlantic overturning circulation and the subpolar gyre for the three model versions. The depth of the NADW overturning cell is taken at the equator. Units are Sv ($= 10^6 \frac{m^3}{s}$) and are taken from the zonally integrated streamfunction (Fig. 9) except for the subpolar gyre (SPG) strength which was calculated as the maximum zonal transport[1].

is shallower as seen from the weaker overturning in the GSR region and north of 65°N (Fig. 9). Due to the dense overflow water, NADW extends to over 2700m in DEEP with the deepest part on the southern slope of the GSR. The presence of the overflow parameterisation overcomes the disconnection of the Nordic Seas and restores the circulation in this region but changes the dynamics. The NADW overturning cell is deeper and stronger in HYDRO than in CTRL. Yet it is shallower than in DEEP, which shows a Nordic Seas overturning cell $\sim 1Sv$ stronger and more intense overflows at 64°N. The stronger overflows in DEEP are compensated by an enhanced downwelling south of the GSR (between 40°N and 64°N) in HYDRO, which results in a comparable maximum of the AMOC (Fig. 9). These findings are in line with Kuhlbrodt et al. (2006), who state that high latitude downwelling is not the primary driving force for the AMOC but upwelling in the tropics and the southern ocean. For this simplified view, a weakening of the downwelling in the Nordic Seas results in an intensification further south (see sect. 2).

In CTRL the deep Atlantic Ocean is lighter at depth as compared to DEEP and denser in shallower layers (Fig. 11, upper right). Deep waters are indeed formed further south, south of Iceland. Furthermore, the Nordic Seas appear lighter. Since the deep outflows must be balanced by the Atlantic inflow at the surface, actually less saline North Atlantic water reaches the high latitudes in CTRL and the Nordic Seas freshen under the action of river run–off and precipitation (fig 11, lower right).

[1]Due to the explicit free surface, our model does not have a well defined vertically integrated (barotropic) streamfunction (see appendix A). Streamlines in following figures are for visualisation purposes only.

Finally, denser water above the GSR is another consequence of weaker the overflows in CTRL. Indeed, dense water formed by surface cooling is not advected out of the region. This does not apply to the rest of the Nordic Seas as the temperature anomaly is particularly strong above the GSR (Fig. 11 middle right). Further north the general freshening dominates the density difference. In the Irminger Sea, around 55°N, water is also lighter in CTRL. Deep convection is generally weaker (Fig. 10) and shifted eastwards from the Irminger Sea into the Iceland Basin. At the same time, we observe a weaker SPG (Table 1). The patterns of the difference in potential temperature and salinity CTRL - DEEP (Fig. 11, centered and lower right) are similar because they are both similarly affected by the weaker deep water formation.

In HYDRO water masses below the level of no motion (compare Fig. 9, $\sim 700m$) are denser than in DEEP throughout the Atlantic Ocean while in shallower layers lighter water is found (Fig. 11, upper left). As before, this must be understood taking into account the deep water formation in the Nordic and Irminger Seas. The Nordic Seas between 65°N and 80°N are more stratified in HYDRO as compared to DEEP. Water masses are lighter in the surface and denser at depth below the sill levels of the GSR (Fig. 11, upper left). This is the effect of the weaker exchange over the ridge. The local overturning circulation is weaker which leads to denser water at depth in DEEP. The surface waters are colder and fresher in HYDRO as a result of a weaker Atlantic inflow. As in CTRL, freshening by river run–off and precipitation becomes more important (fig 11, lower left). Due to the less intense saline inflow dense water formation requires a stronger local cooling in HYDRO (see Fig. 11, centered left). The potential temperature at depth is lower in HYDRO but still higher than in the climatology (see Montoya et al. (2005) and appendix C). This indicates that the strong exchange over the GSR as observed in DEEP (Fig. 9, upper) is not very realistic. It entails a strong ventilation of the Nordic Seas and hence too warm and saline water masses in this region especially at depth.

The most prominent difference between HYDRO and DEEP is the dense water column around 55°N (Fig. 11, upper left). It reaches from the surface to the bottom of the NADW at 2500 m. It is related to the stronger subpolar gyre in HYDRO (Fig. 13) that increased its transport by roughly $10Sv$ to $28Sv$ as compared to DEEP. It is associated to a temperature dipole that can be seen in the temperature difference

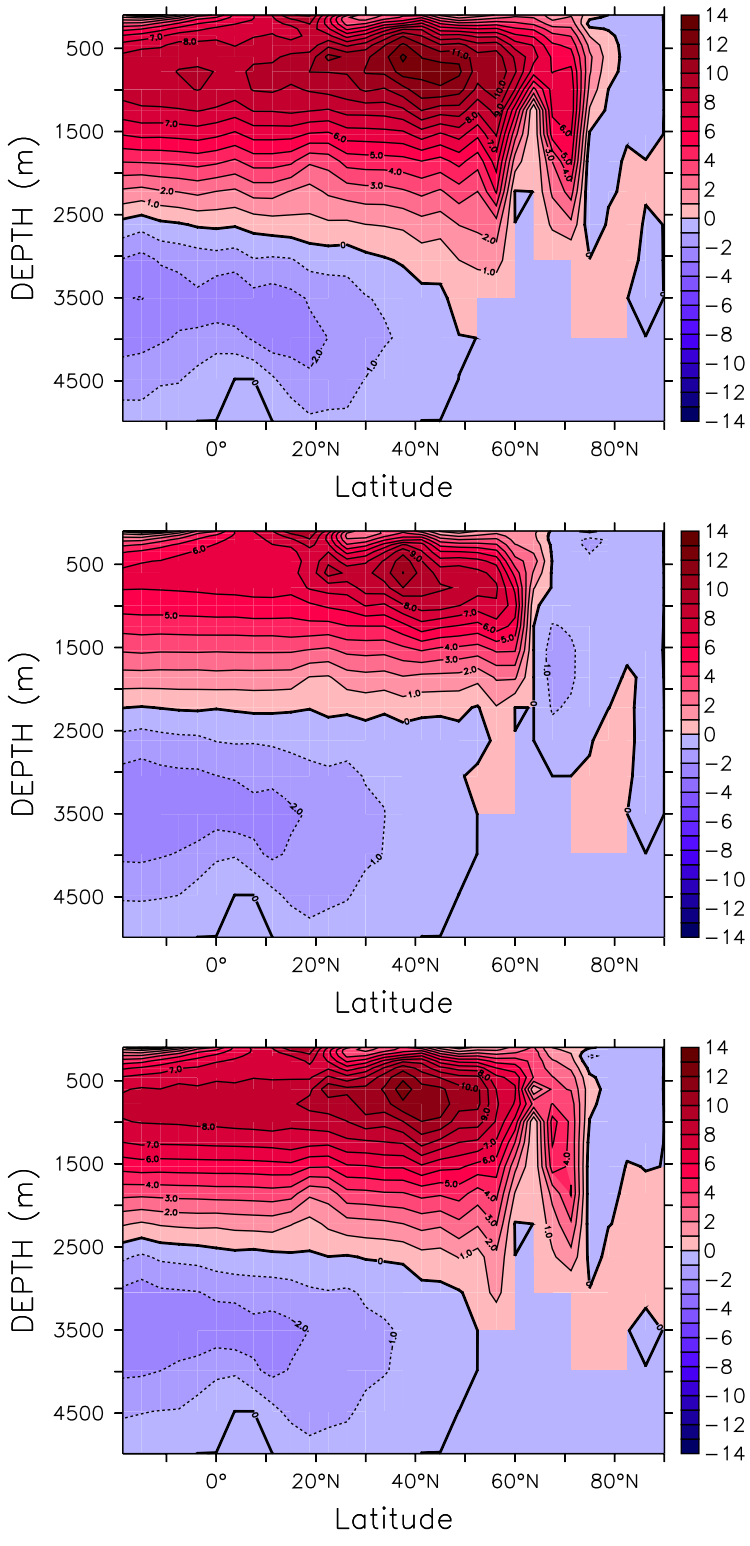

Figure 9: Atlantic streamfunction for DEEP (upper), CTRL (middle) and HYDRO (lower). Due to the GSR barrier (64°N), no exchange occurs between the North Atlantic and the Nordic Seas in CTRL. No meridional circulation is observed inside the Nordic Seas and it is weaker than in the other two experiments in the entire Atlantic. In HYDRO, circulation in the Nordic Seas is weaker than in DEEP as well as the exchange over the GSR.

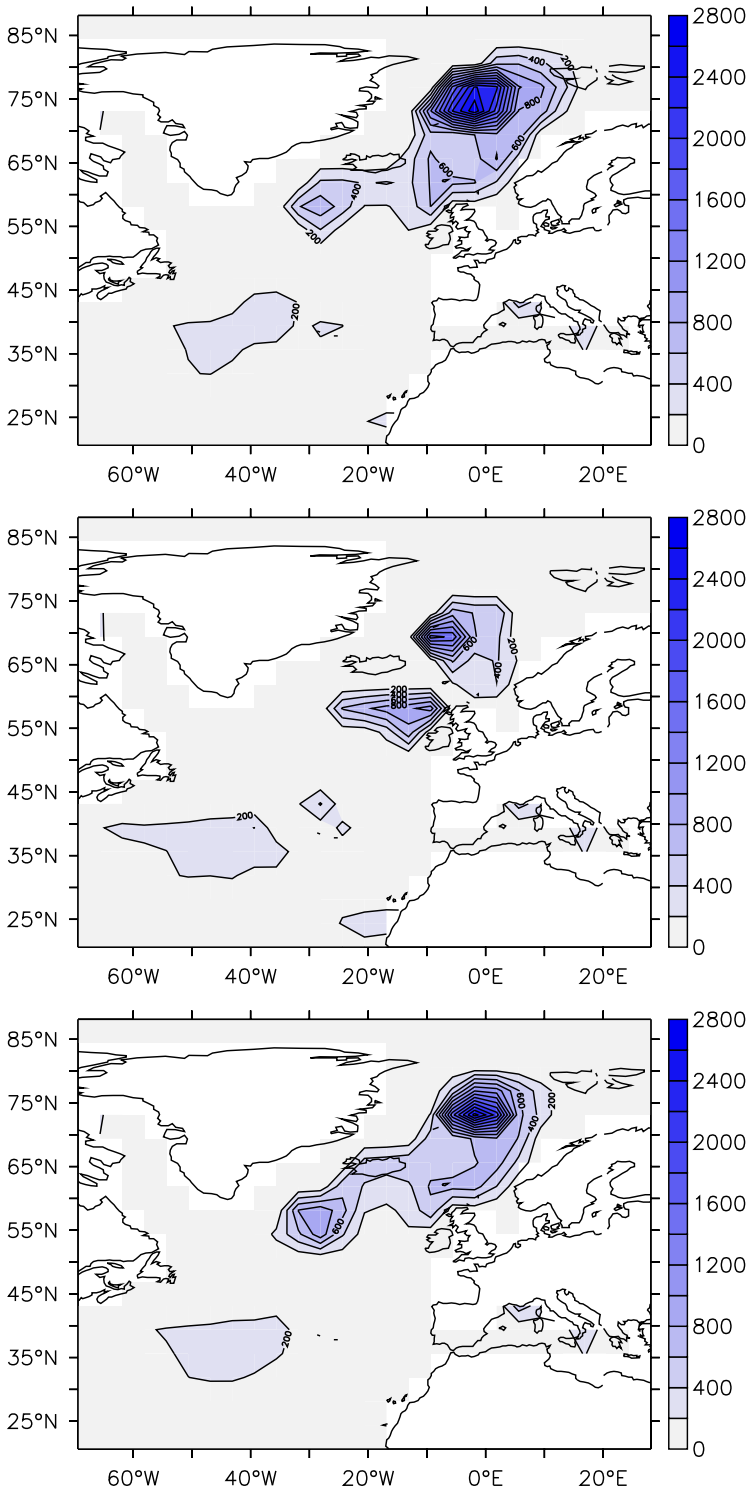

Figure 10: Maximum winter mixed layer depth for DEEP (upper), CTRL (middle) and HYDRO (lower). While in CTRL convection is weaker, DEEP and HYDRO give similar results. In these two model versions convection takes place north of the GSR (64°N) and in the Irminger Basin southwest of Iceland. Note that our model does not show Labrador Sea deep convection due to the coarse resolution (Montoya et al., 2005).

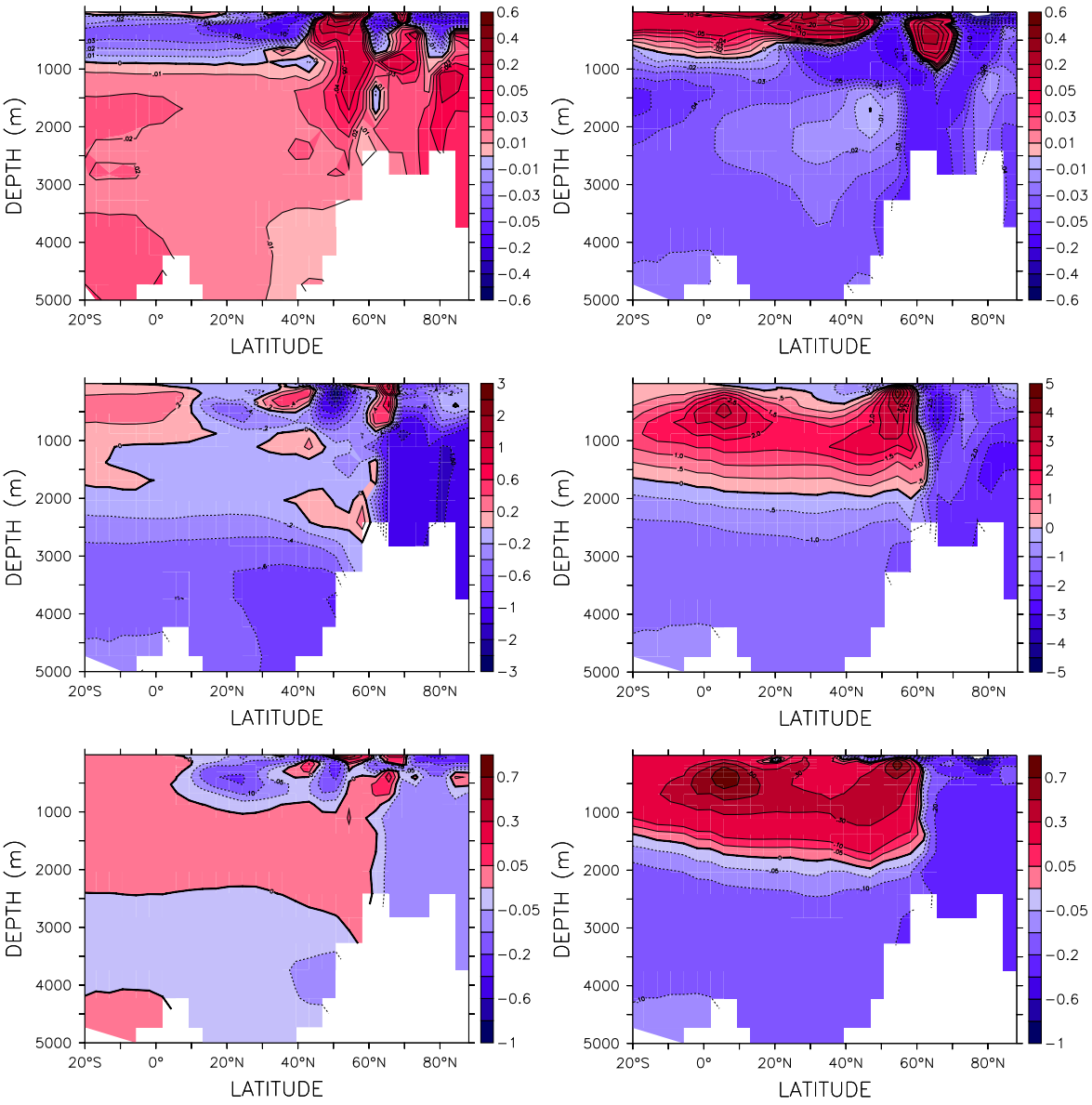

Figure 11: Differences in the tracer distribution, HYDRO - DEEP on the left, CTRL - DEEP right. The upper panels shows the potential density ($\frac{kg}{m^3}$), the centered the temperature (K) and the lower panels the salinity (psu). The sections have been averaged zonally from 50°W to 30°E excluding the Mediterranean.

from the surface down to 1000 m (figure 11, centered left), centered at 55°N, which is also the centre of the SPG (Fig. 13). The gyre circulation increases from 18 Sv to 28 Sv (Tab. 1) in HYDRO as compared to DEEP, while it remains at the same location (Fig. 13). The same pattern can also be found in the salinity section but here it is disrupted by a plume of less saline water in HYDRO that overlays the effect of the gyre (Fig. 11, lower left). These observations are consistent with a stronger SPG as here more warm and saline North Atlantic water reaches the northern side of the gyre and colder, fresher water of Arctic origin is advected to the South. The sea surface elevation drops by more than 0.5 m in the centre of the SPG (Fig. 14).

This change in water mass distribution by the stronger SPG represents changes in the meridional heat transport (Fig. 12). The heat transport by the horizontal gyre circulation is stronger in the south of the GSR for HYDRO while the transport of heat by zonally averaged flow is stronger in DEEP. This is the result of the weaker meridional overturning in this region in HYDRO because of the shallower passages (at 64°N) while on the other hand more volume and heat transport occurs in a horizontal circulation. This can also be seen in the heat flux into the ocean (figure 13). In HYDRO the ocean takes up more heat in the south–west of the SPG and loses more at its north–eastern side.

7 Performance with a bottom boundary layer parameterisation

After passing the GSR, the overflow currents rapidly flow along the slope of the submarine ridge and Greenland, respectively (see sect. 3.2). The representation of such density driven downslope flows is another problem in ocean modelling, especially for coarse resolution models because the discretisation of the bottom topography transforms the even slopes into staircases. Continuous downslope flow thus is replaced by a series of horizontal advection and turbulent mixing. This results in unrealistically high mixing rates, the so–called numerical entrainment and the initial dense water signal is lost before it reaches the bottom.

In order to overcome this problem, a wealth of parameterisations have been proposed. One is the bottom boundary layer (BBL) parameterisation for a den-

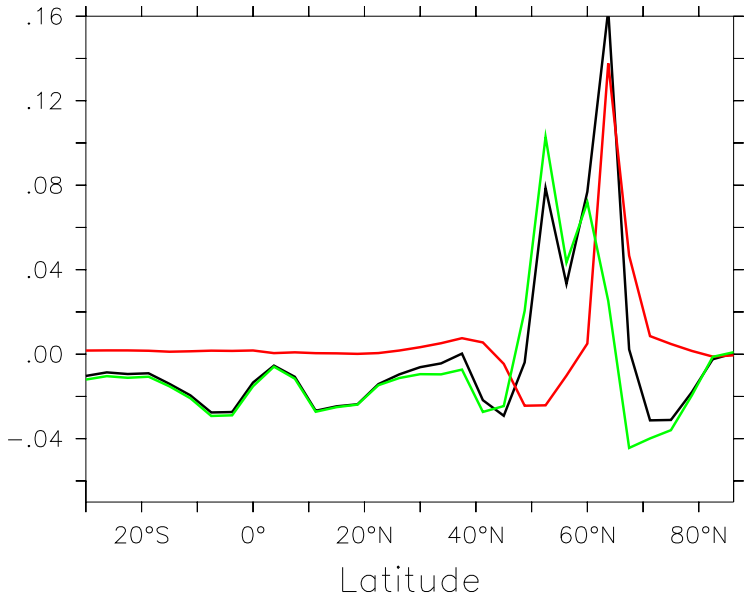

Figure 12: Difference in the northward heat transport, HYDRO - DEEP (black), decomposed into the fraction transported by the AMOC (zonal transport, red) and the gyres (azonal transport, green).

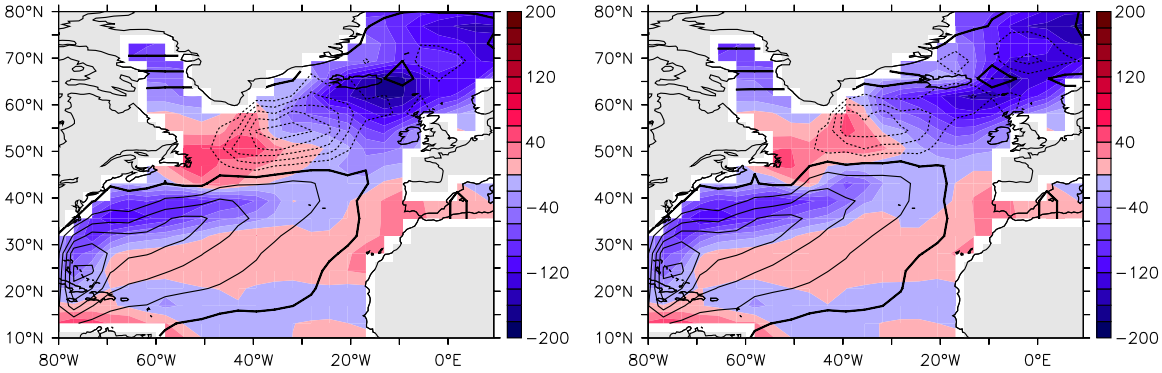

Figure 13: Heat flux into the ocean, negative values correspond to an oceanic heat loss. With the enhanced SPG in HYDRO more heat is transported from the south–west end of the gyre to the north–east (compare with Fig. 12). Left for HYDRO, right for DEEP, units are $\frac{W}{m^2}$. Contours: streamlines of the vertical integrated circulation.

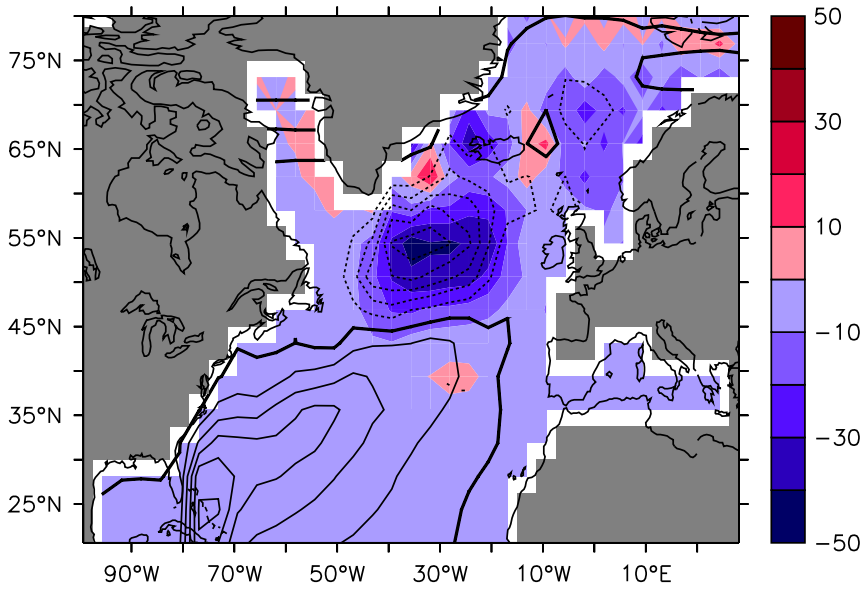

Figure 14: Difference in sea surface elevation, HYDRO - DEEP (cm). The stronger circulation causes a maximal deviation of ∼0.5 m is in the centre of the gyre as can be seen in the streamline contours (for HYDRO).

sity driven downsloping flow by Campin and Goosse (1999). In combination with the hydraulic overflow parameterisation it shows a weaker and shallower Atlantic overturning (experiment CGHYDRO). The maximum transport is ∼2 Sv less as in the model version with overflow parameterisation only. The GSR overflows are of comparable strength as well as the Nordic Seas overturning cell (Fig. 15). The NADW is significantly lighter than in the experiment without BBL while for the Antartic bottom water (AABW) in the Atlantic basin the density difference is less pronounced. The Nordic Seas are also lighter (Fig. 16 upper). For the North Atlantic we observe a reduction of the density gradient at 1000 m depth between a southern region from 20°N to 30°N and a northern from 40°N to 60°N of $\sim 0.05 \frac{kg}{m^3}$. According to Griesel and Maqueda (2006) this explains the reduction of about 2 Sv of the meridional overturning. The meridional pressure difference balances a westward geostrophic flow that feeds the southbound deep Atlantic western boundary current. Concerning the density difference in the Nordic Seas, we find that the effect of the parameterisation is to freshen and warm the high northern latitudes (Fig. 16 middle and lower).

Hence the BBL parameterisation weakens the AMOC because of the presence

of less dense water masses in the Nordic Seas and consequently lighter overflows. This results in a less dense NADW while processes determining the density of the AABW are not altered.

We carried out these experiments with a lower value for the vertical diffusivity ($0.1 \times 10^{-4} \frac{m^2}{s}$ instead of $0.2 \times 10^{-4} \frac{cm^2}{s}$). This does not change the general circulation fundamentally but does for example slightly weaken the AMOC (for a detailed discussion, please refer to Mignot et al. (2006)). Thus, the model version with overflow parameterisation only can not be compared with the results presented in section 6.

Kösters et al. (2005) found similar results for the same BBL parameterisation. While in their model the AMOC does not weaken, the parameterisation neither stabilises it in a anomalous freshwater flux scenario.

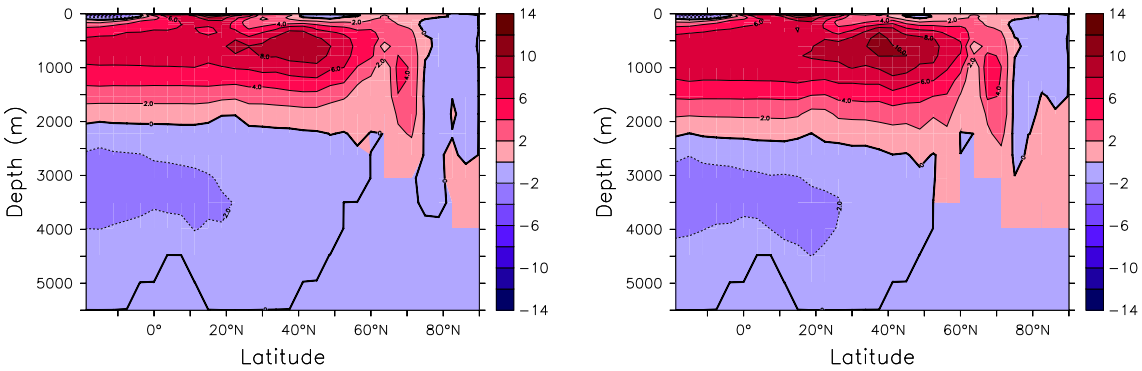

Figure 15: Zonally integrated streamfunction of the Atlantic Ocean (in Sv). Left: For the model version with hydraulic overflow and bottom boundary layer parameterisation applied (CGHYDRO). Right: For the experiment with only the overflow parameterisation. Note that these experiments have been made with a lower value for the vertical diffusivity ($0.1 \times 10^{-4} \frac{m^2}{s}$ instead of $0.2 \times 10^{-4} \frac{cm^2}{s}$). The AMOC is weaker for lower vertical diffusivity and these figures can thus not be compared with those in section 6.

We applied another bottom boundary layer parameterisation which is a generalisation of the approach by Beckmann and Döscher (1997) (Gnanadesikan, 1997). Unfortunately, the present implementation in our model is numerically unstable.

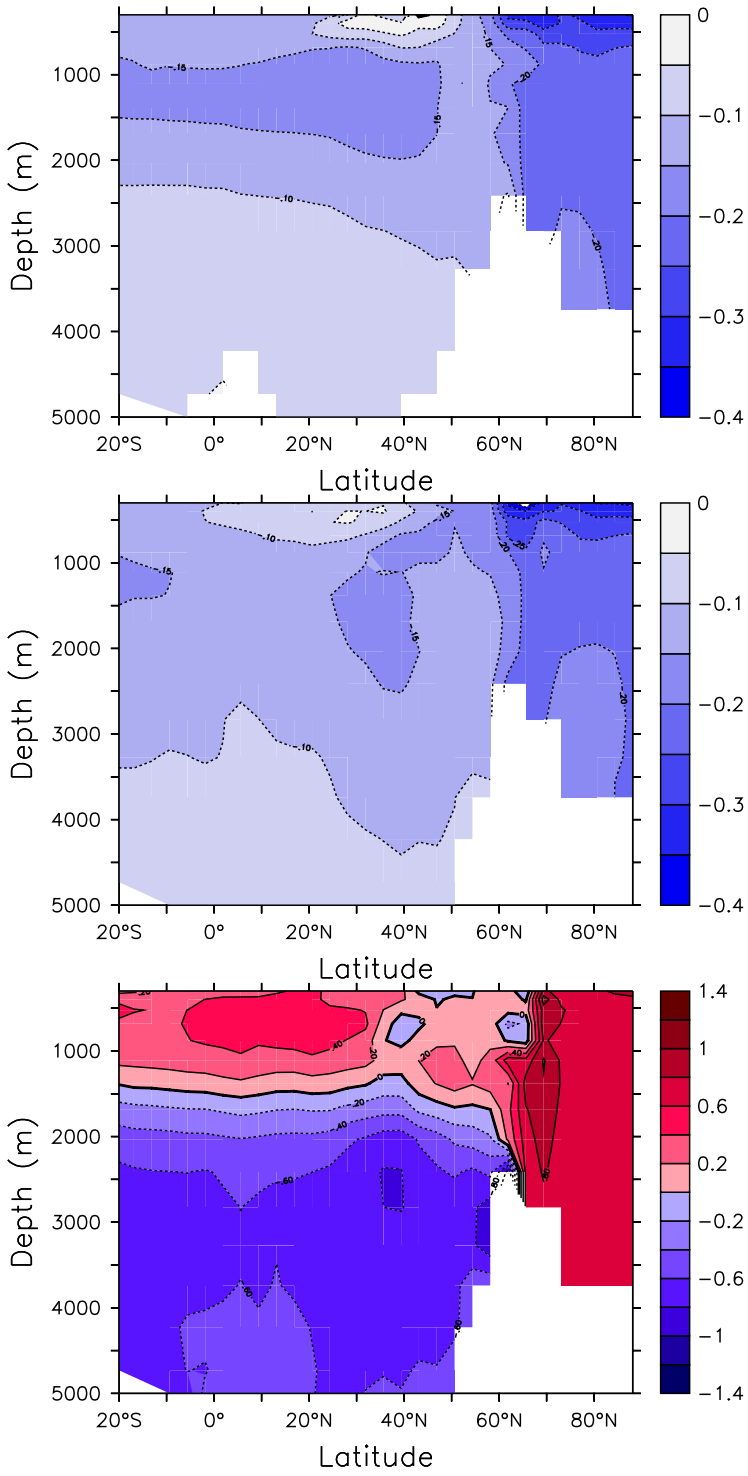

Figure 16: Difference in tracer distribution in the Atlantic Ocean averaged zonally from 50°W to 30°E excluding the Mediterranean. Positive values indicate excess in the experiment with overflow parameterisation and bottom boundary layer parameterisation (BBL) over the version with the overflow parameterisation only. Upper: Potential density ($\frac{kg}{m^3}$), middle: Salinity (psu), lower: Temperature (K).

8 The hydraulic overflow parameterisation as a tracer transport

While the BBL by Campin and Goosse (1999) parameterises a downslope transport as a tracer flux, the hydraulic overflow parameterisation represents a source term in the momentum equations, i.e. a volume flux. Because our model employs a staggered Arakawa B-grid (Arakawa, 1966; Bryan, 1969), this set–up is possibly not the most efficient in order to advect dense water masses over a sill and deep into an adjacent basin. First, the alternating order of tracer and velocity grid points results in only half of the overflow transport being in the tracer bottom cell. Thus only half of it is subject to the BBL parameterisation. Secondly, it is a known problem of the overflow parameterisation that with a strong volume transport applied into only one velocity grid point the horizontal compensation of the flow is challenged. Up– and downstream of the parameterised passages down– and upwelling can be observed, respectively.

As a possible solution to this problem we implemented a different combination of the two parameterisations. The downslope transport was still calculated as proposed by Campin and Goosse (1999) everywhere in the entire domain but the two passages of the GSR. There we maintained the hydraulic transport equation (1) of Kösters et al. (2005) but did not apply the result as a source in the momentum equation but in the same way as the downslope transport, that is in the tracer transport (experiment COMB). For comparison, we implemented the original overflow transport estimate as a tracer transport without the BBL parameterisation (HYDTRA).

A common problem of these two model versions is that the Nordic Seas overturning is weaker than in HYDRO (Fig. 17a, b). The density in this region is lower (Fig. 17c, d). We observe a similar general freshening of the Atlantic in COMB as before for CGHYDRO which is the main reason for the lighter water masses (Fig. 17e). The BBL parameterisation must create a salinity sink (not salt sink) outside the Atlantic Ocean. Due to the weaker cross GSR transport, less heat is transported to the Nordic Seas, which are colder in COMB than in HYDRO. South of the GSR, the Atlantic is warmer in turn.

For HYDTRA we observe a stronger AMOC than for CGHYDRO with a max-

imum of 11 Sv at 35°N. The Nordic Seas meridional circulation is stagnant except for a weak overturning near the GSR (Fig. 17b). This is the principal difference to the unparameterised model version CTRL (Fig. 9 middle). Due to this weaker circulation the Atlantic overturning cell is warmer and more saline while the deep ocean and the Nordic Seas are colder and fresher (Fig. 17f, h). In the potential density distribution we observe denser surface and lighter deep water than in HYDRO. North Atlantic deep water formation takes place south of the GSR which leads to lighter water in this region as compared to HYDRO.

The most important outcome of the study of CGHYDRO and HYDTRA is that it is crucial for the overflow parameterisation to employ a volume flux. In the original implementation by Kösters et al. (2005) not only the overflows are parameterised but also the Atlantic inflow. In our model this inflow is primarily a compensation for the overflow transport, Ekman transport plays a minor role (see also sect. 6). So the overflows do act as the driving force for the AMOC in this region. This does not question vertical diffusion or upwelling in the southern ocean as the main physical driving mechanisms for the entire AMOC (Kuhlbrodt et al., 2006) because the Nordic Seas downwelling is only one downwelling branch of at least two (see sect. 2). The overflow strength determines the proportion of the AMOC that enters the Nordic Seas.

9 Dynamics of the subpolar Atlantic Ocean

9.1 Vorticity balance in the subpolar gyre

In order to understand the differences in SPG circulation, we have to revise its dynamics. The contours plotted in figure 13 are derived from the field $M = \int_{-H}^{0} dz \int dx v(x, y, z)$. Note that this field does not define an exact streamfunction due to the free surface implemented in our model (see appendix A). It however approximates the horizontal transport. Thus, our first step is to derive an equation for the vertically integrated transport from the primitive equations.

$$f M_x \equiv f \int_{-H}^{0} dz\, u. \tag{2}$$

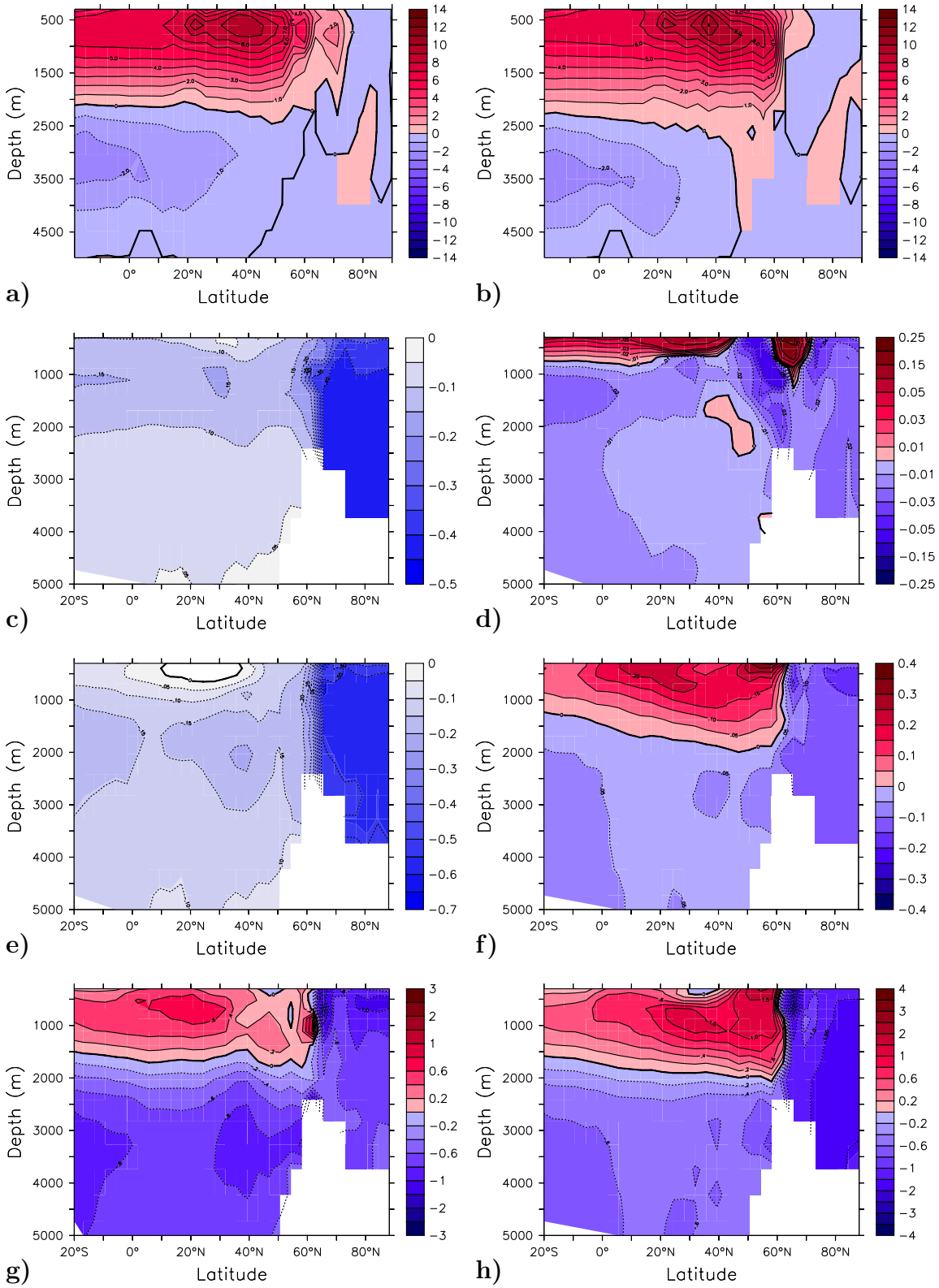

Figure 17: a, b: Zonally integrated streamfunction of the Atlantic (Sv). c – h: Scalar properties as deviations from HYDRO. c, d: potential density ($\frac{kg}{m^3}$); e, f: Salinity (psu); g, h: Temperature (K). Experiment COMB (left), HYDTRA (right).

We choose the zonal transport as it depends on meridional tracer variations and hence allows us to detect the influence of the overflows, as will become clear later. Consider the time independent momentum equation in zonal direction,

$$fu = -g\,\partial_y\eta - \partial_y \int_{-z}^{\eta} b'dz' + \rho_0^{-1}\,\partial_z\tau_{zy}, \tag{3}$$

with the average density ρ_0, sea surface elevation η, gravitational acceleration g, Coriolis parameter f and the stress term τ_{zy} for a meridional force acting on the horizontal surface. b denotes the buoyancy

$$b = b(x,y,z) \equiv g\,\frac{\rho-\rho_0}{\rho_0}; \qquad b' = b(x,y,z'). \tag{4}$$

We integrate over the entire water column in order to obtain the depth integrated transport M_x. We neglect bottom friction and small contributions from the uppermost layers and choose limits from $-H$ to 0:

$$\begin{aligned} fM_x &\equiv f\int_{-H}^{0} dz\,u \\ &= -Hg\partial_y\eta - H\partial_y\int_{-H}^{0} b\,dz - \partial_y\int_{-H}^{0} z\cdot b dz + \frac{\tau_{0y}}{\rho_0} \qquad (5)\\ &= -H\partial_y P_b + \partial_y\Phi + \frac{\tau_{0y}}{\rho_0}, \qquad (6) \end{aligned}$$

with

$$\begin{aligned} P_b &\equiv g\eta + \int_{-H}^{0} dz'\,b' \qquad (7)\\ \Phi &\equiv \int_{-H}^{0} dz \int_{-H}^{z} dz'\,b' = [z\int_{-H}^{z} dz'\,b']_{-H}^{0} - \int_{-H}^{0} dz\,zb = -\int_{-H}^{0} dz\,zb. \qquad (8) \end{aligned}$$

We split the buoyancy term in equation (3) into two parts in order to simplify the integration:

$$\int_{-z}^{\eta} b'dz' = \int_{-H}^{\eta} b'dz' - \int_{-H}^{z} b'dz'. \tag{9}$$

We identify $\rho_0 P_b$ as the bottom pressure and $\rho_0\Phi$ as the potential energy at depth H. For the meridional transport we yield similarly:

$$-fM_y = -H\partial_x P_b + \partial_x \Phi + \frac{\tau_{0x}}{\rho_0}. \tag{10}$$

Now, we cross differentiate equation (6) and equation (10) and add them up to obtain

$$\begin{aligned} \mathbf{M} \cdot \nabla(\frac{f}{H}) &= \\ M_x \partial_x(\frac{f}{H}) + M_y \partial_y(\frac{f}{H}) &= H^{-2}(\partial_y H \partial_x \Phi - \partial_x H \partial_y \Phi) \\ &\quad + \partial_x \left(\frac{\tau_{oy}}{\rho_0 H} \right) - \partial_y \left(\frac{\tau_{ox}}{\rho_0 H} \right). \end{aligned} \tag{11}$$

The right hand term is the vertically integrated mass transport across contours of constant planetary potential vorticity ($\frac{f}{H} = const$). The bottom pressure term was eliminated and the two remaining terms represent the joint effect of baroclinicity and relief (JEBAR) and the surface wind stress curl. The concept of JEBAR was first described by Sarkisyan and Ivanov (1971). Mertz and Wright (1992) give some physical interpretations, Cane et al. (1998) critique. Equation (11) can also be interpreted as a vorticity balance in which transport across $\frac{f}{H}$ contours is driven by vorticity input from the wind and the JEBAR. Note that not only lateral density variations but also a sloping topography are crucial. In a flat ocean the JEBAR vanishes.

9.2 Dominance of the JEBAR term

For the analysis of our model we will use the expression for the vertically integrated zonal transport (equation (6)). As we are interested in the changes of the SPG circulation, we focus on the terms equivalent to the vorticity creating terms in equation (11). Thus, we neglect the bottom pressure term in (6). Actually we do not observe differences in this term between DEEP and HYDRO. Among the remaining two terms of equation (6) we find differences in the wind stress term to be negligible (fig. 18, top right).

This allows us to focus on the second term of equation (6). We did not change the topography outside the sills of the GSR so that changes in the JEBAR contributing

to the SPG must be due to the changed density distribution alone (eq. (11)). The difference in the zonal transport contribution $f^{-1}\partial_y\Phi$ (eq. (6)) is shown in the upper left of figure 18, the difference of the vertically integrated zonal transport derived from the model's simulated velocities on the lower left. Positive values indicate a stronger eastwards transport in HYDRO as can be observed in the southern half of the SPG. On its northern side, a stronger westwards transport conveys more water to the west. Note that large changes in JEBAR and the observed transport from the velocities are confined to the SPG region only. Contours are for the stream lines of the SPG in HYDRO and demonstrate the spatial agreement with the gyre. In figure 18, lower right $f^{-1}\partial_y\Phi$ has been zonally averaged over the centre of the gyre (40°W to 20°W) and then meridionally integrated in northern direction in order to obtain a measure of the gyre strength difference. This term explains a difference in the gyre transport (HYDRO - DEEP) of roughly $10Sv$. We compare it to the red curve of the vertically integrated zonal transport derived from the model's simulated velocities (Fig. 18, lower left). The two curves show a good agreement excepting near the Greenland coast where the neglected effect of friction becomes dominant. They begin to diverge at 56°N, the latitude of Cape Farewell in our model. The comparison confirms the difference of the maximum transport of $\sim 10Sv$ and thus, that the main difference between HYDRO and DEEP is due to the JEBAR.

9.3 Role of the overflows

The influence of the GSR overflows on the SPG has been reported repeatedly in previous model studies for example, from Roberts and Wood (1997), Redler and Böning (1997) and Penduff et al. (2000), who indicate that the outflow of cold water from the Nordic Seas enhances the SPG circulation. Our results generally support this view: in our experiment CTRL the SPG is considerably weaker than in DEEP (Table 1). Yet, we want to modify it on the basis of the findings mentioned above. In order to understand how baroclinicity drives the SPG we return to the second term in equation (6) and its interpretation as potential energy. The contour plot in figure 19 shows a range of density isolines zonally averaged over the SPG centre (40°W – 20°W). Their slope can be used to evaluate qualitatively the derivative of the potential energy that enters equation (6) (second term) and drives the SPG. It

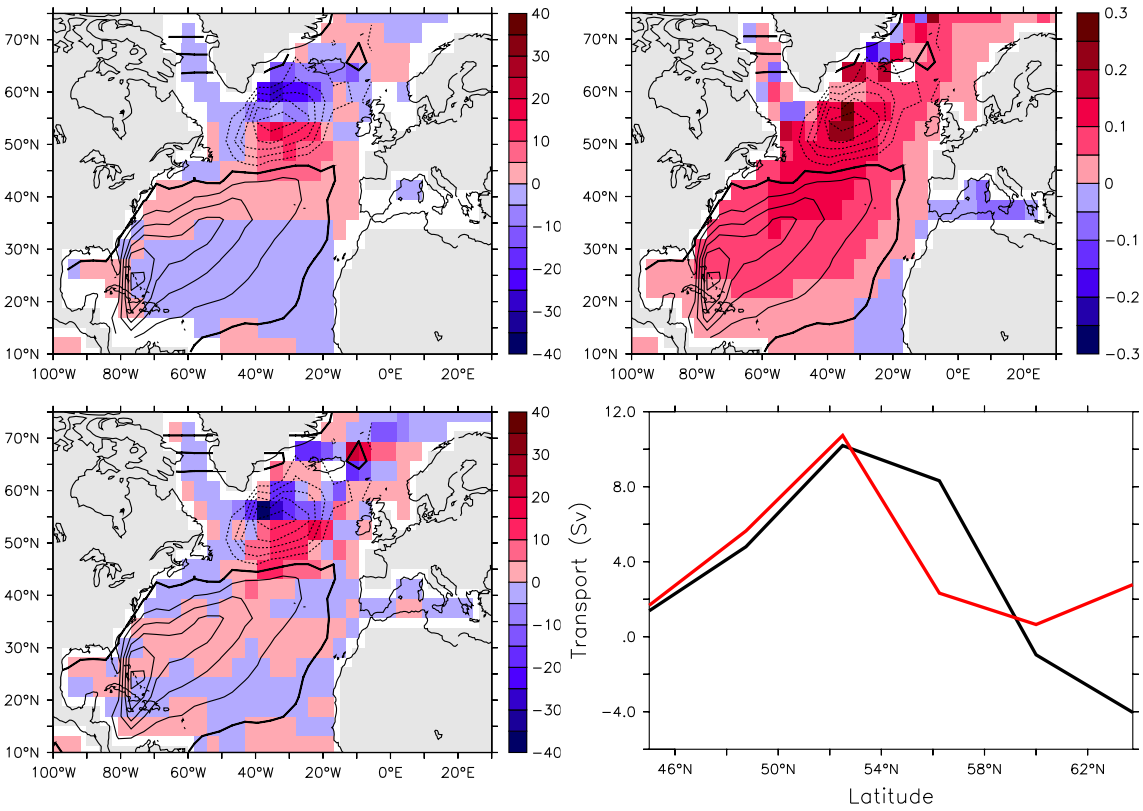

Figure 18: Differences HYDRO - DEEP in the vertically integrated, zonal transport. Positive values indicate eastwards transport (m^2/s), contours are stream lines of the vertically integrated transport in HYDRO and demonstrate the spatial agreement of the changes with the SPG. Upper left: Vertically integrated zonal transport as computed from $f^{-1}\partial_y\Phi$, lower left: Vertically integrated zonal transport as derived from the model's simulated velocities, upper right: Difference in the vertically integrated zonal transport due to changes in the wind stress. Differences in wind stress are small as compared to those in the JEBAR forcing and do not reproduce the gyre structure, in contrast to the differences due to baroclinicity. Bottom right: Vertically integrated transport as shown in left panels, zonally averaged over the the gyre centre (40°W – 20°W) and meridionally integrated in order to obtain a measure of the gyre strength difference. The black curve corresponds to the transport derived from the density field (upper left), the red one to the simulated velocities (lower left). The curves disagree near the Greenland coast due to the neglected friction terms in equation (6). The maximum value in the gyre centre is in good agreement (10 Sv).

is more intense in HYDRO as seen from the stronger outcropping of the isopycnals. Concerning the resulting transport in zonal direction, figure 19 further shows the derivative of the integrand of equation (8), which is proportional to the meridional density gradient weighted by depth ($z \cdot \partial_y \rho$). It is positive for HYDRO over the whole depth of the southern half of the SPG south of 55°N and negative in the north. The separation is sharp and located in the centre of the gyre. In DEEP we do not see the same vertical separation between the positive and negative contribution of JEBAR to the zonal transport. In the upper layers, the steeper rise of the isopycnals between 40°N and 55°N is the cause for the more intense eastwards transport in HYDRO in the southern half of the SPG. On the northern side of the gyre the isopycnal gradient is negative in HYDRO, resulting in an enhanced westwards transport. In DEEP the isopycnals neither rise as much nor fall notably. While the isopycnal maxima in HYDRO are all at the same latitude, they are displaced to the south with increasing depth in DEEP. The deeper isopycnals are smoother but the density derivative gains significance with increasing depth due to the weight of the depth coordinate z. At these depths, the most important difference is the strong positive driving in DEEP on the southern slope of the GSR around 60°N, which cumbers the cyclonic gyre transport. On the contrary, the positive driving seen between 50°N and 55°N in HYDRO is weaker in DEEP and leave way to a stronger and more extend negative cell centered at 44°N.

The positive driving from the JEBAR in the overflow region in DEEP is the consequence of the local increase of density on the southern slope of the GSR in relation to the open North Atlantic. A thorough comparision of the isopycnals shows that the slope water is not much denser in DEEP than in HYDRO and that the change of the gradient is due to the lighter water in the SPG centre further south. The weaker negative gradient above 800 m is explained similarly: the density in the gyre centre is the main difference between the two model versions. The density in the gyre centre corresponds to a stronger deep convection in the Irminger Basin (fig. 10 and 11).

Due to the stronger SPG heat and salt transport intensify (Fig. 12). For reasons we will discuss in detail in the following section these results in a cooling of the gyre's centre and the stronger transport of salinity into the subpolar region (Fig. 20). As recently found by Hátún et al. (2005) a more intense gyre circulation also

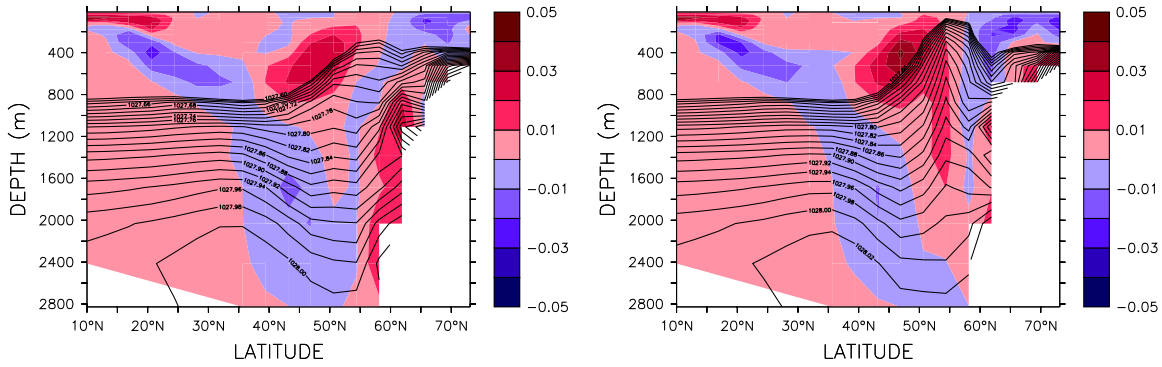

Figure 19: Meridional density gradient weighted by depth, $z \cdot \partial_y \rho$, averaged over the SPG centre (40°W to 20°W). It provides a mesure of the zonal transport due to the JEBAR (see equation (6)). Left: DEEP, right: HYDRO. The contours show a certain range of the corresponding isopycnals. With the stronger gyre in HYDRO, more isopycnal outcropping is seen and the domed structure is maintained over the entire depth. The vertical separation between the positive (eastwards) and negative (westwards) forcing is also more pronounced. Intense overflow transport in DEEP causes a eastwards transport on the GSR slope between 800m and 2500m. Units are arbitrary as we focus on the sign only.

decreases the salinity of the Atlantic inflow into the Nordic Seas so that the salt remains in the region and the gyre becomes not only cooler but also more saline (Fig. 20). The result is the observed increase in density (Fig. 11 upper panels). We found that the SPG differences between HYDRO and DEEP are due to the steeper gradient of the density isolines, the isopycnals, and ultimately that this gradient is changed more by the increase of density in the gyre's centre than the decrease at its rim. Hence, a large portion of the notable intensification of the SPG in HYDRO is the result of an auto–intensification by internal mechanisms. The overflows are important because they control the SPG from outside.

In a study of decadal variability of the North Atlantic circulation, Eden and Willebrand (2001) report a strong correlation between the mixed layer depth in the gyre centre and the strength of the SPG in their high resolution model. They also argue with JEBAR as they can exclude variations in wind stress and other contributions are small. This would add another external control mechanism to the SPG which is linked to what in our case is an internal feedback. Our results support this finding but, as the related processes are limited to decadal time scales they are not taken into account here. Our atmospheric submodel does not resolve decadal variability.

As Eden and Willebrand (2001) we did not calculate the contribution of the JEBAR to the absolute strength of the SPG, but only to the intensification due to a change in the overflow transport. Still, this difference (Fig. 18 (upper left)) confirms the findings of Myers et al. (1996) that especially the eastern part of the gyre in the Irminger and Iceland Basins is JEBAR controlled, which leads to a westwards transport along contours of constant planetary potential vorticity, that is along the continental slope of Greenland and North America. Note that the fact that the SPG does not follow the slope into the Labrador Sea in our model is owed to the coarse resolution and the resulting lack of deep water formation in this region (Montoya et al., 2005).

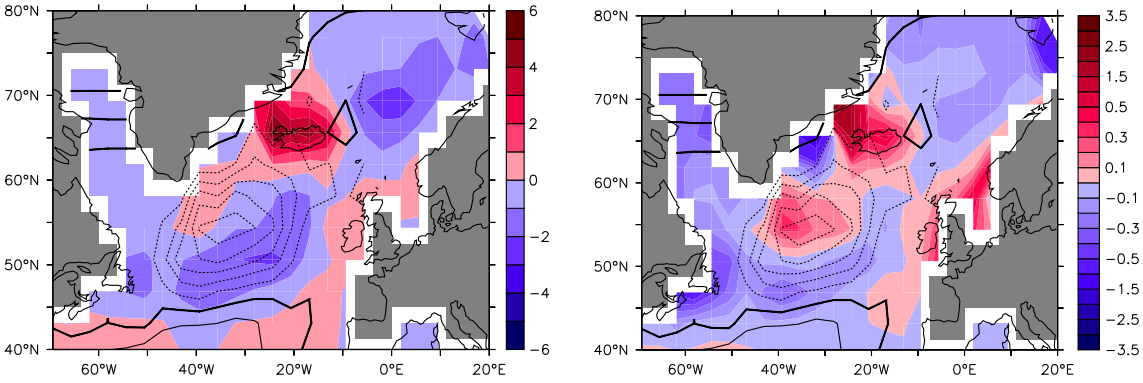

Figure 20: Temperature (left) and salinity (right) differences HYDRO - DEEP in the North Atlantic and Nordic Seas, averaged over the upper 1000 m. Contours: stream lines for HYDRO. The centre of the SPG is colder and more saline in HYDRO which results in a higher density (compare with fig. 11). We also observe a stronger deep convection in this region in HYDRO (Fig. 10).

10 Bistability of the subpolar gyre, stabilising effect on the North Atlantic region

As discussed earlier, the experiment with unconstrained and artificially deep GSR passages, DEEP, exhibits a equilibrium transport of 18.4 Sv, which is not consistent with present day observations (Bacon, 1997; Read, 2001; Clarke, 1984). We assumed the intense overflow transport to debilitate the SPG circulation although we identified JEBAR as the primary difference and that the major difference in JEBAR comes from processes that are controlled by the SPG itself (Fig. 19). The justification was that the overflows provide an external control while the processes inside the gyre can only act as intensification. We can further argue with the mere fact that there is no other difference between HYDRO and DEEP than the hydraulic overflow parameterisation including localised changes in bottom topography that do not affect the SPG. In this section we want to analyse the involved mechanisms more in detail for the unparameterised model DEEP.

Surface wind stress is believed to have a strong influence on strength and variability of the SPG (Curry et al., 1998; Böning et al., 2006), but it has also been reported repeatedly that part of the gyre circulation is controlled by baroclinic adjustments

and therefore the density structure in the region (Myers et al., 1996; Penduff et al., 2000; Eden and Willebrand, 2001). Recent measurements show a strong freshening of the region in the last four decades (Blindheim et al., 2000; Dickson et al., 2002; Curry and Mauritzen, 2005) and satellite observation of sea surface elevation suggest a rapid reduction in SPG strength since 1992 (Häkkinen and Rhines, 2004). Further, simulations with a high resolution climate model suggest that the Atlantic inflow into the Nordic Seas is strongly modulated by the strength of the SPG south of the Greenland-Scotland ridge (Hátún et al., 2005). On the other hand, we found in section 9 that the overflows affect the SPG via the baroclinic forcing.

The addition of 0.05 Sv of anomalous freshwater flux into the Nordic Seas for a period of 50 years switches the circulation into a stronger state with ∼27 Sv of SPG strength, comparable to HYDRO (Tab. 1). Further integration for 950 years shows that this mode is stable. Application of a negative anomaly of 0.1 Sv for another 50 years in the same region switches the system back into the original state.

In our model the bistability can be understood as follows. The SPG is at the center of three positive feedback loops which cause the nonlinear response of the system and are responsible for the two stable states (Fig. 21). First, a stronger SPG transports more heat to northern high latitudes (red curve in fig. 22a). Therefore the center of the gyre gets colder (Fig. 23a and 24a). This increases the density gradient between the center and the relatively light rim and strengthens the gyre (T-feedback, Fig. 21). Secondly, a stronger gyre transports more tropical saline water into the subpolar region. As shown previously in a high-resolution model for this situation (Hátún et al., 2005), less tropical waters are then transported to the Nordic Seas, more of it recirculates in the SPG, making the centre more saline (Fig. 23b, 24b). This again increases the core density of the gyre and therewith its strength (S-feedback, fig. 2).

In addition to these self sustaining positive feedbacks (hereafter: internal feedback loops, compare fig. 21), there exists the interaction with the flow over the Greenland-Scotland ridge. The stronger SPG reduces the salinity of the Atlantic inflow which results in a weaker deep water formation in the Nordic Seas and ultimately a weaker overflow over the GSR (black curve in fig. 22b). Downwelling south of the ridge consequently increases (red curve in fig. 22b). Therefore the density at the northern rim of the SPG decreases (red curve in fig. 22c), because it is now fed

by relatively light water that is formed south of the ridge as opposed to the dense overflow waters. Note that we have not succeeded to trigger the transition between the two states by application of a surface flux directly onto the SPG. This highlights the significance of the external feedback and hence of the overflows on the subpolar gyre circulation.

The causal chain of events in the simulations of figure 22 is related to these three feedbacks. The first application of the positive freshwater anomaly causes an immediate reduction in overflow strength (fig. 22b) which yields a rapid decline in density along the Greenland-Scotland ridge, i.e. at the northern rim of the SPG (fig. 22c). This triggers the external positive feedback loop (fig. 21). The associated reduction in SPG volume transport (fig. 22a) affects the two positive internal feedbacks and causes the main increase in gyre strength. The time lag of the internal feedbacks can be clearly seen in the delayed response of the density at the center of the gyre (fig. 22b). The negative freshwater anomaly shows the same succession of events only that the overflows are enhanced in response to the densification of the surface water and the external feedback is triggered negatively, leading to a reduction in SPG strength.

The two stable states of the SPG are associated with different North Atlantic climate states. In contrast to previous studies (Häkkinen, 2001), the maximum of the overturning stream function does not vary between the two states. The increased heat transport of a stronger gyre, however, enhances surface air temperature by up to 2 K south of Greenland (Fig. 25) and sea surface elevation is more than 0.25 m lower in the stronger state (Fig. 26). These differences are consistent with the observed changes due to the hydraulic overflow parameterisation in section 6 (Fig. 13 and 14). For the same increase in SPG strength as compared to the weak SPG mode HYDRO shows a larger difference in the sea surface elevation. However, the time evolution of the sea surface elevation difference is in good agreement with the SPG strength for DEEP.

The integrated precipitation into the Nordic Seas from the NCEP–NCAR reanalysis varies between 0.09 Sv and 0.17 Sv (Fig. 27). The largest variation ocurred in the early 1960's with a difference of 0.08 Sv between 1959 and 1965. The amplitudes of the variations are comparable to the freshwater pulse applied to our model. However, they show no persistent trend in the last decades. A possible melting of

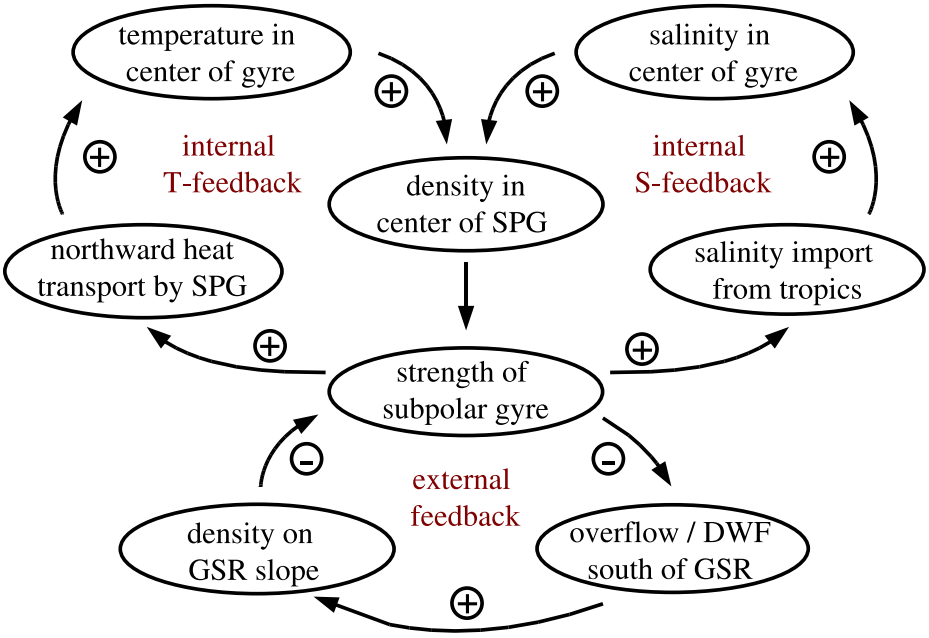

Figure 21: Feedback mechanisms of the subpolar gyre. The upper loops represent the internal temperature and salinity mechanisms that yield the auto–intensification, the lower mechanism contains the GSR overflows and provides external control on the system.

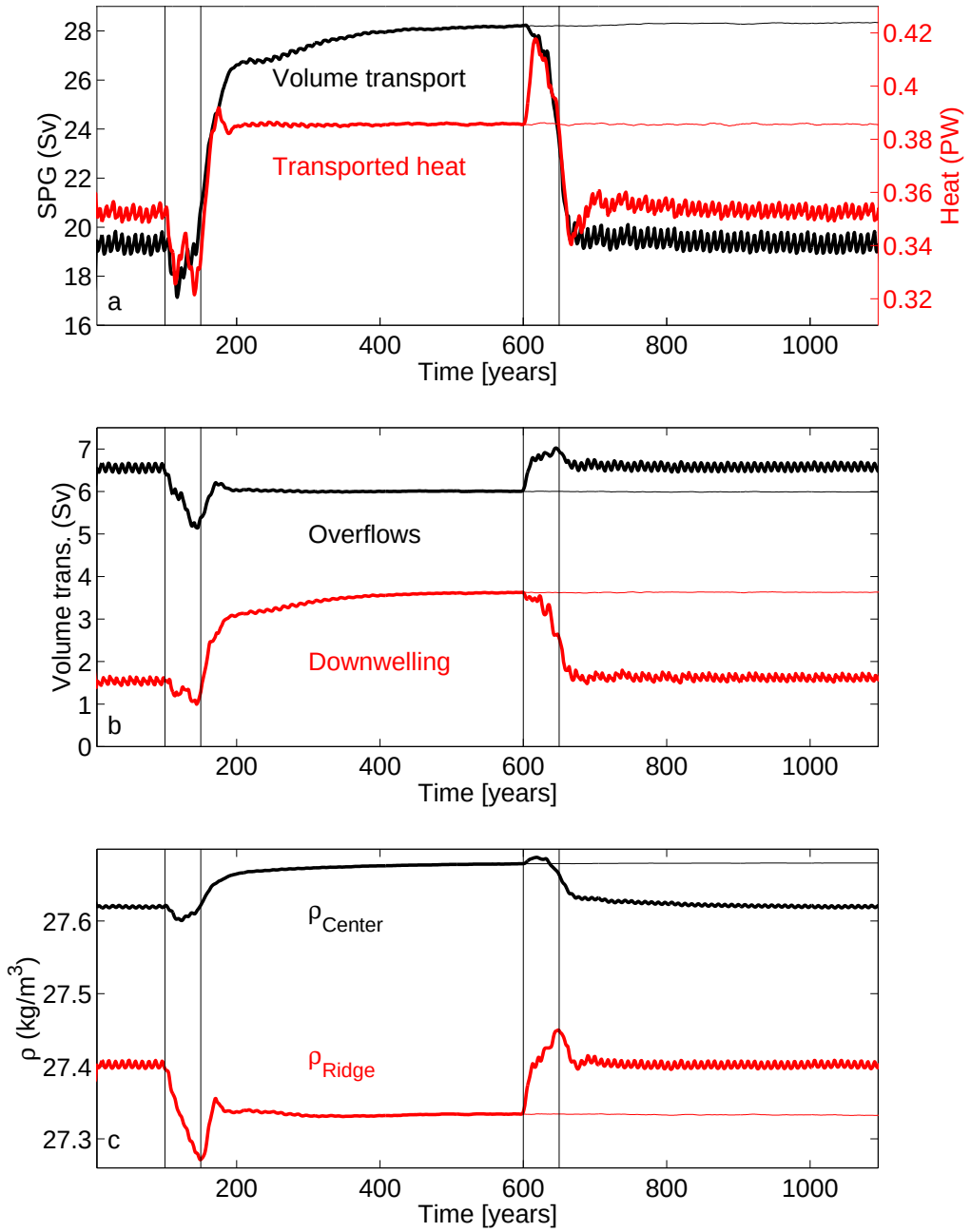

Figure 22: Time evolution of the main dynamic quantities of the feedback loops in figure 21. The vertical lines indicate the beginning and end of the freshwater pulses into the Nordic Seas. The thick curves show the evolution of the experiments with both pulses applied. The faint curves show that the model stays in the strong circulation mode if only the first pulse is applied.

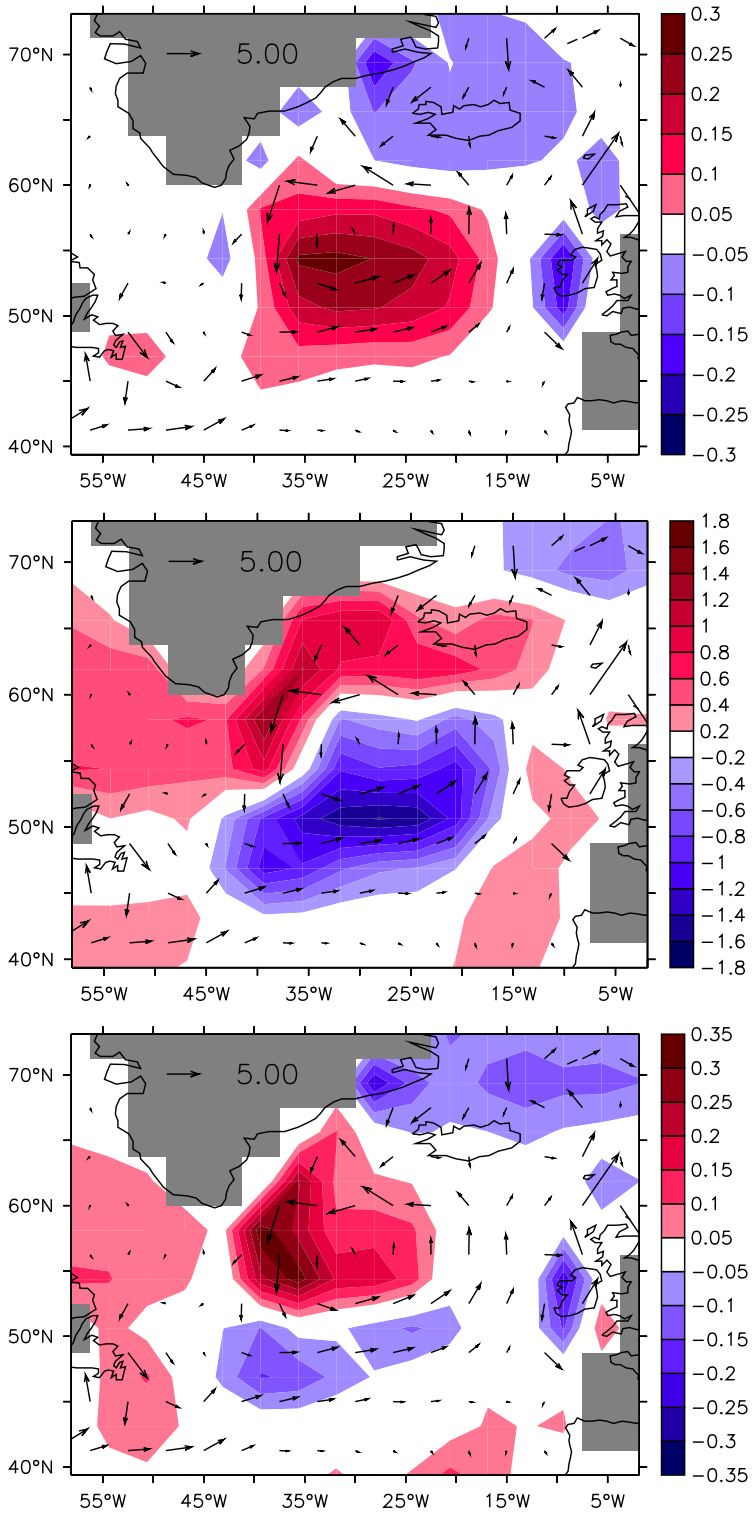

Figure 23: Difference strong minus weak SPG-state (averaged over upper 1000 m): temperature (upper, in K), salinity (middle, in psu) and density (lower, in $\frac{kg}{m^3}$). Vectors show vertically integrated horizontal velocities of the strong SPG mode. The density at the centre of the stronger SPG is enhanced both due to increased salinity and decreased temperature.

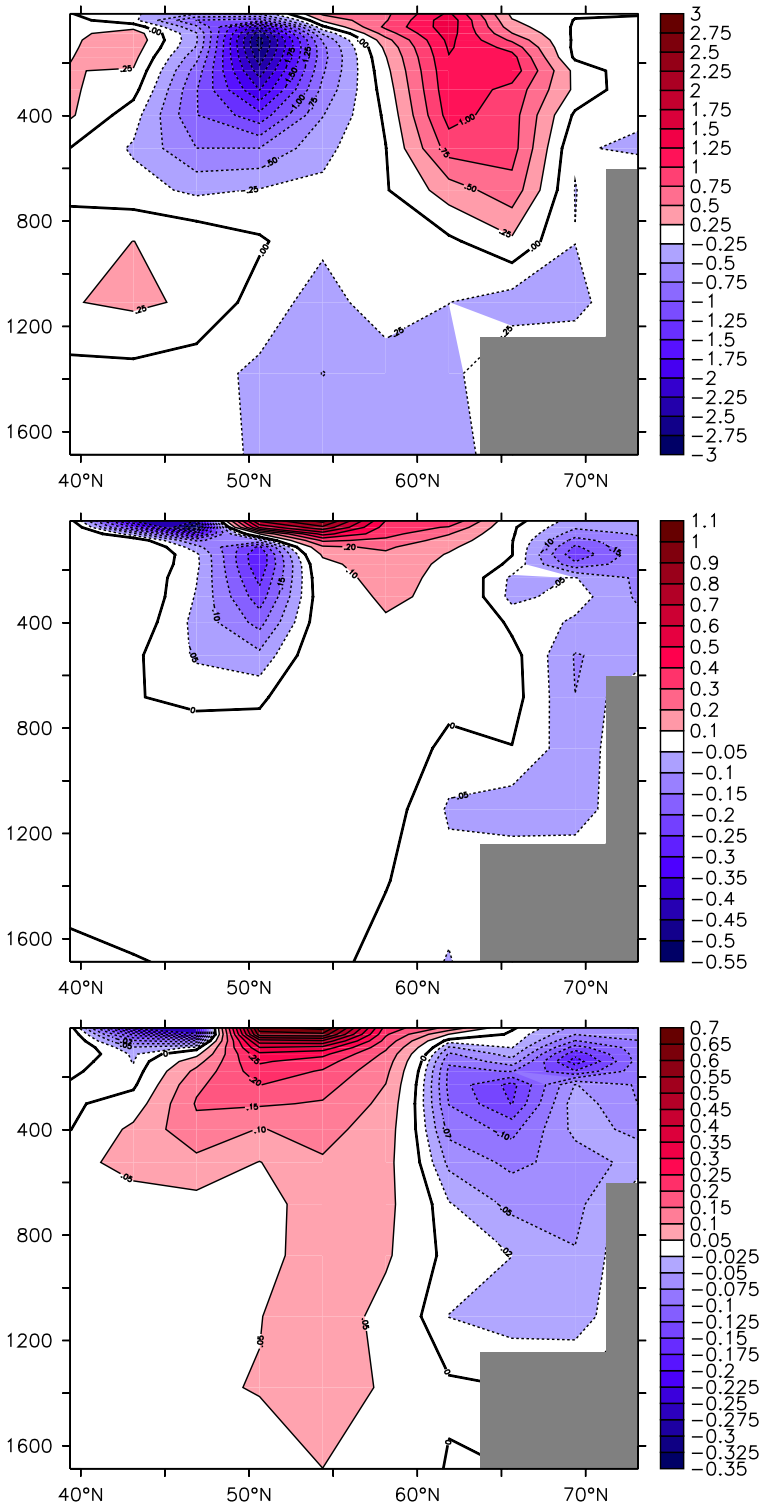

Figure 24: Difference strong minus weak SPG-state (meridional section averaged between 45W and 15W): temperature (upper, in K), salinity (middle, in psu) and density (lower, in $\frac{kg}{m^3}$). The centre of the stronger SPG is denser due to reduced temperatures in the subsurface and higher salinities in the entire water column. Mainly freshening decreases the density along the Greenland–Scotland slope.

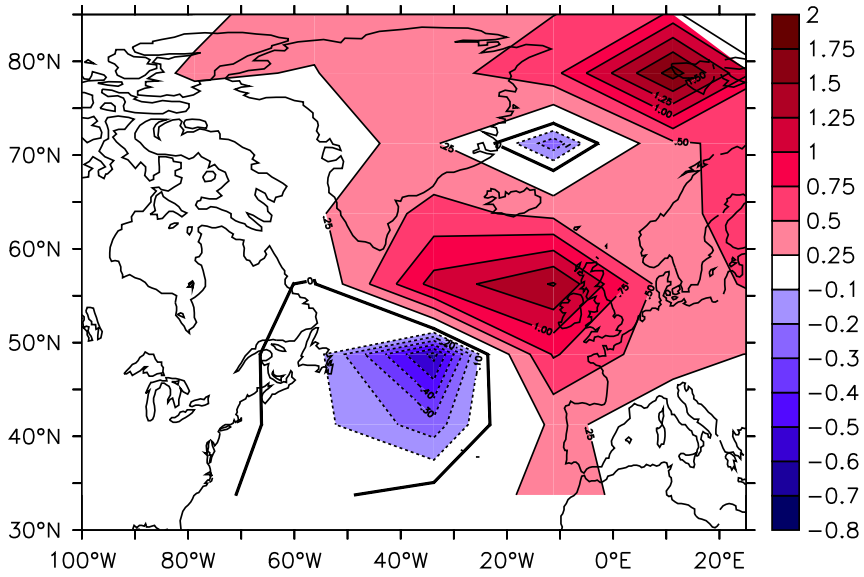

Figure 25: Difference in surface air temperature in the North Atlantic regioin (K). The increased heat transport of a stronger gyre enhances surface air temperature by up to 2 K south of Greenland.

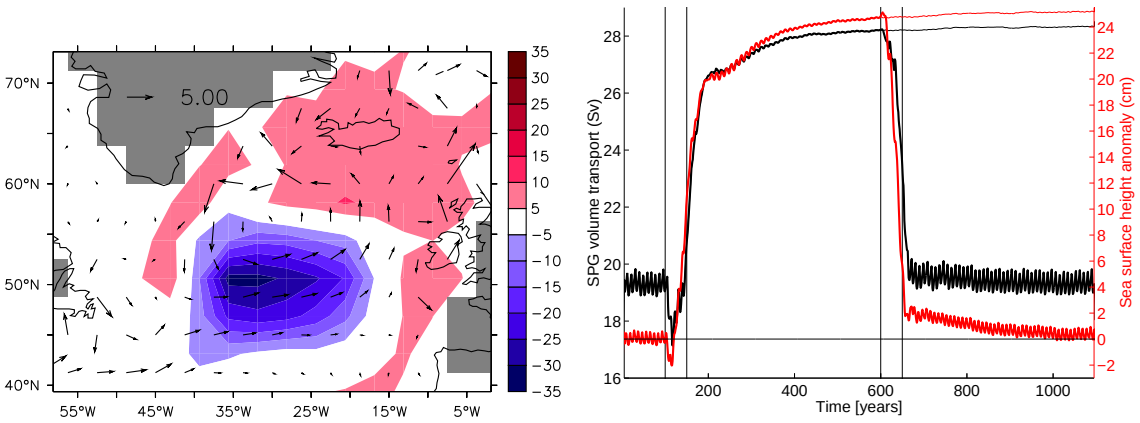

Figure 26: Difference in sea surface elevation. Left: Difference between strong and weak SPG state (cm). Note that the maximal deviation between the states does occur south of the center of the gyre, which is given by the velocity field of the strong SPG mode (arrows). Right: Time series of the strength of the gyre and the maximum deviation of sea surface elevation in the subpolar region from the standard simulation. The vertical lines denote the duration of the freshwater pulses.

the Greenland ice sheet due to global warming is able provide such a trend. It holds enough freshwater to yield a continuous flux of 0.1 Sv for one millennium.

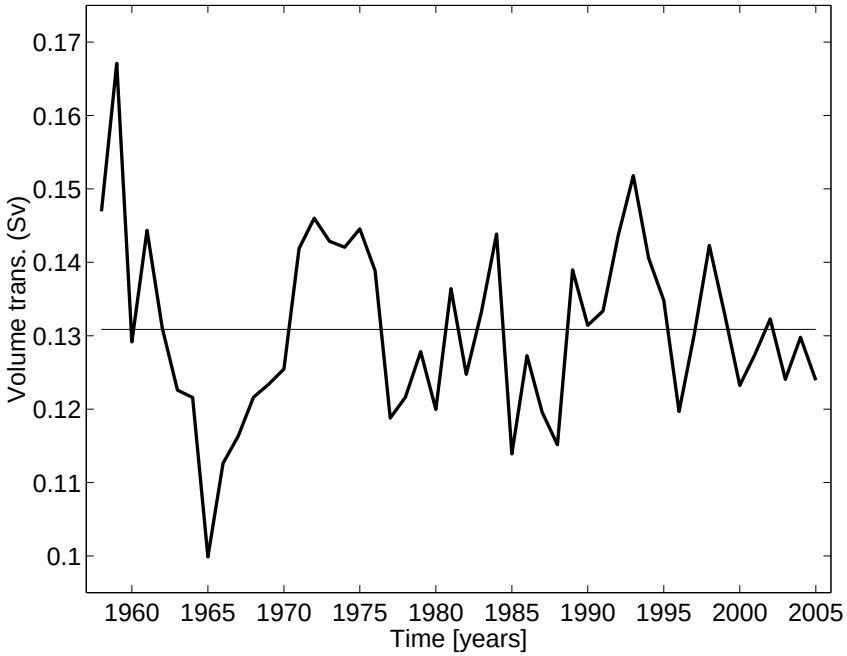

Figure 27: The integrated precipitation into the Nordic Seas from the NCEP–NCAR reanalysis (Kalnay et al., 1996). Variations range from 0.09 Sv to 0.17 Sv.

The experiments show that the internal feedback mechanisms do not initiate themselves but need to be triggered by a change in the overflow/downwelling ratio. The stronger SPG mode in DEEP is dynamically similar to HYDRO and the scalar properties also compare well (Fig. 20 and 23). Due to a fundamentally different representation of the overflow transport in HYDRO, only the strong SPG mode is stable. The overflow parameterisation stabilises the North Atlantic region.

11 Response to a continuous anomalous freshwater flux and the parameterisations influence on the stability of the AMOC

Both model versions, with parametrised GSR overflows by hydraulic constraints and with artificially deepened passages give good results for present–day climate. This

is an important finding because the involved dynamics are fundamentally different, but must not be overestimated as both model versions have been adjusted to this particular climatology.

In order to understand how the hydraulic overflow parameterisation changes the stability of the oceanic circulation, we performed a series of experiments with anomalous freshwater flux to the North Atlantic. The anomalous freshwater flux is applied as a negative saltflux between the latitude band from 20°N to 50°N in the Atlantic Basin. For a detailed stability analysis of the AMOC in DEEP including the response to different forcing regions see Gölzer et al. (2006). Weakening of the maximum of the AMOC with increasing freshwater flux is similar for HYDRO and DEEP (Fig. 29). On the other hand the anomalous overflow strength behaves differently. While in DEEP almost the entire weakening of the overturning is also seen in a weakening of the overflows, overflows are much more stable in HYDRO.

This can be understood through the mechamism driving the AMOC. These upwelling processes are not directly related to the deep water formation in high latitudes. In a simplified view, sinking merely defines the shape of the AMOC (Kuhlbrodt et al., 2006). Actually the upwelling process depends on the precise composition of the deep water mass, at least if we assume that vertical diffusion processes in the tropical Atlantic play a role. This composition depends on the region and volume of the sinking process. The tropical Atlantic is less stratified in CTRL (Fig. 11 upper right) and the AMOC is about 20% weaker (Tab. 1). However, as HYDRO and DEEP both show sinking in the Nordic Seas, vertical density differences are less and so are those in maximum AMOC strength. For this example the simplified view is a good approximation. In this view we can argue that if water masses cannot sink in one region, the sinking process shifts to another region in order to maintain the same volume transport. The overflow transport is a good estimate for the deep water formation in the Nordic Seas. Water masses advected in the AMOC that do not sink there must sink between 40°N and 64°N in the North Atlantic (see Fig. 9). We see that for high anomalous freshwater fluxes (above 0.2Sv) the overflows in DEEP stop and the entire deep water formation takes place south of the GSR (Fig. 29). This does not occur in HYDRO where the overflow transport is relatively stable over the presented interval. Consequently the sinking in the North Atlantic region is more sensitive to the anomalous freshwater flux as

can also be observed in the mixed layer depth (Fig. 29, right and 28).

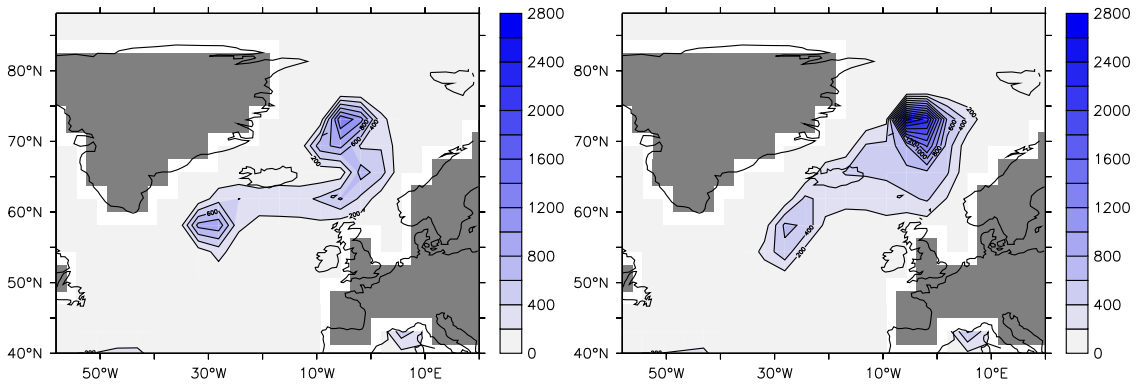

Figure 28: Maximum winter mixed layer depth (m) for an anomalous freshwater flux of 0.2 Sv, left: DEEP, right: HYDRO. The convection in the Nordic Seas is deeper for HYDRO, while south of the GSR DEEP shows a deeper mixed layer.

In HYDRO the overflows have to cross the GSR at shallower depths than in DEEP (Fig. 30), which has implications for the transport of salinity and heat. In the experiments with 0.2 Sv anomalous freshwater flux the overflow strength is equal in HYDRO and DEEP (Fig. 29). Nonetheless salinity changes in the Nordic Seas as compared to the respective nonperturbed experiments are weaker in HYDRO because of the Atlantic inflow. In HYDRO it enters the Nordic Seas as a surface current while in DEEP it flows at intermediate depths (Fig. 30). Thus it advects more saline water to the high latitudes. It also transports more heat. Sea–ice in DEEP reaches further south and tends to close the Nordic Seas along the GSR at 64°N but not in HYDRO (Fig. 31). The surface air temperatures differ by ~ 2 K from the equilibrium in HYDRO and more than 6 K in DEEP in the experiment with 0.2 Sv anomalous freshwater flux.

Due to its bistable nature addressed before the SPG circulation intensifies in DEEP with an anomalous freshwater forcing of 0.05 Sv, even with continuous hosing. The same applies for the stronger forcing rates but here the negative effects become more important (Fig. 29, right).

We carried out another series of experiments with anomalous freshwater flow for the model version with the DEEP topography but starting from the strong SPG state discussed in section 9 (Fig. 29, red curves). It shows that the stability of the North Atlantic circulation depends on the initial strength of the SPG. For

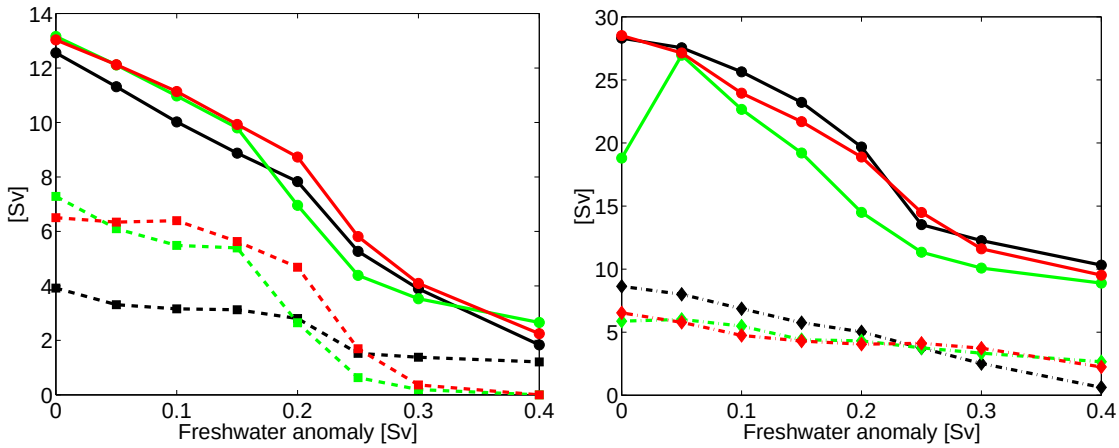

Figure 29: Changes in the dynamics with a salt flux applied to the latitude band between 20°N and 50°N, black: DEEP, green: HYDRO, red: DEEP in the strong SPG mode before the continuous freshwater flux. Left: Maximum overturning strength (solid) and overflow volume (dashed) as function of the freshwater anomaly. Right: Maximum subpolar gyre transport (solid) and the sinking the NA region between 40°N and 60°N (dash–dotted). Because the overflow transport and hence the deep water formation in the Nordic Seas is more stable in HYDRO the NA sinking is more sensitive to the anomalous freshwater flux. For DEEP, the SPG increases with moderate hosing in because of the bistability discussed earlier. The experiments that were initialised from DEEP with a freshwater pulse into the Nordic Seas in order to obtain the strong SPG mode before application of the continuous anomalous freshwater flux (red) show a different sensitivity. A stronger SPG stabilises the meridional overturning circulation in our model. Experiments are indicated by the markers, lines are for visualisation only.

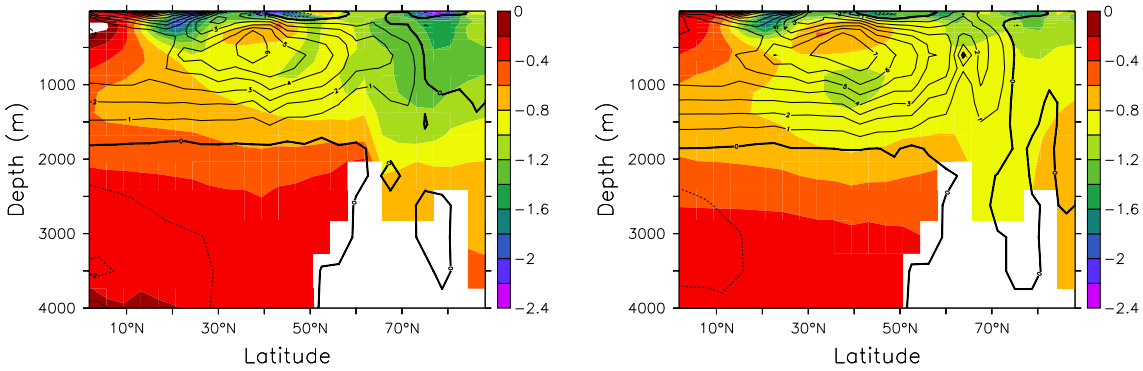

Figure 30: Salinity changes in the experiments with 0.2 Sv anomalous freshwater flux into the North Atlantic compared to their respective equilibrium experiment, units are PSU, DEEP on the left, HYDRO right panel. In DEEP the Nordic Seas freshen more than in HYDRO although the overflow transport is equal in both experiments (Fig. 29). This is due to the shallower Atlantic Inflow in HYDRO seen in the contours (intervall 1 Sv).

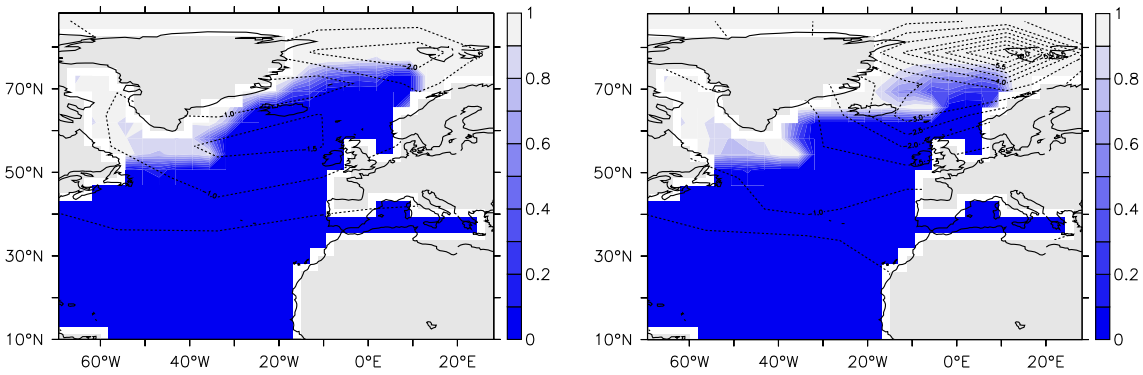

Figure 31: Maximum winter sea–ice fraction for HYDRO (left) and DEEP (right) with anomalous freshwater flux (0.2 Sv). Contours show the surface air temperature difference to the respective unperturbed experiment (in K). Note that in DEEP sea–ice tends to close the Nordic seas even with an ongoing circulation below the surface (Fig. 30). In HYDRO the overflow transport is equal in strength but due to the overflow parameterisation in shallower depths.

moderate anomalous forcing between 0.05 Sv and 0.15 Sv the two DEEP versions show similar maximum overturning and overflows. For freshwater fluxes between 0.15 Sv and 0.3 Sv the experiment with the stronger initial SPG shows stronger AMOC and overflows, the SPG circulation is also stronger than in the experiment with initial weak SPG (Fig. 29, right). In our model, a stronger SPG stabilises the meridional overturning circulation.

12 Conclusions and Discussion

An overflow parameterisation for the Nordic Seas by hydraulic constrains was implemented in a coarse resolution climate model. We can confirm the finding of Kösters et al. (2005) that this parameterisation overcomes the problem of a missing exchange over a realistically represented GSR. Simulations with the unparameterised model version with realistic topography (CTRL) yielded unsatisfactory results.

In the parameterised model version HYDRO, weaker and denser overflow water masses mix with more ambient water in the North Atlantic than the strong but relatively light unparameterised overflows in the model version with artificially deepened passages (DEEP) (Fig. 8). This results in relatively small differences in density in the Atlantic basin as compared to the unparameterised version with realistic topography (CTRL) (Fig. 11). On the other hand, the Nordic Seas ventilation is weaker in HYDRO which permits the formation of denser water masses. The stronger exchange across the GSR in DEEP results in warmer and more saline water in the deep Nordic Seas. Temperatures and salinities in this basin are closer to observed values in HYDRO and suggest that the GSR region is better represented in HYDRO for the present–day climate (Fig. 32) (Levitus, 1982).

With the parameterised overflows the mass exchange, as seen in the zonally integrated stream function, is less than the overflow transport reported from observations (Fig. 9) (Hansen and Østerhus, 2000). This does not necessarily indicate an incorrect representation as the parameterised transport becomes partially compensated by other cross GSR flows. Actually, it is close to observational values. One limitation of the presented parameterisation is that it simulates the volume transport but not other possibly important characteristics of the overflows as for example

entrainment or interactions with the ocean bottom. It also does not parameterise the descent of the dense water plume along the GSR slope. A bottom boundary layer parameterisation (BBL) could resolve some of these problems. In our model none of the tested BBL parameterisations was able to generate an acceptable large scale oceanic circulation.

A notable difference is found in the strength of the SPG, which is 28 Sv in HYDRO and hence is about 10 Sv stronger than in DEEP. This is a reasonable value according to measurements by Bacon (1997), who found a gyre transport of 25-27 Sv. Clarke (1984) derived a higher value of 33.5 Sv from another section across the SPG. High resolution models tend to show an even more vigorous circulation of order 40–50 Sv (Treguier et al., 2005).

In the analysis of the underlying mechanisms we found the JEBAR to be the dominant difference between DEEP and HYDRO. This is in agreement with Greatbatch et al. (1991) and Myers et al. (1996) who found the SPG entirely controlled by JEBAR. Penduff et al. (2000) came to the same conclusion and state that in their model JEBAR clearly dominates all contributions able to generate transport across $\frac{f}{H}$ isolines.

Eden and Willebrand (2001) report a strong correlation between the mixed layer depth in the gyre centre and the strength of the SPG on decadal time scales in their high resolution model, which they also relate to the JEBAR. Our results support this finding but as the related processes are limited to decadal time scales they are not taken into account here. Our atmospheric submodel does not resolve decadal variability.

We identified two mechanisms that control the SPG strength through JEBAR. The first one is an auto–intensification of the gyre due to deep water formation in its centre that depends on the gyre related heat and salt transport. Because the influence of atmospheric variability as suggested by Eden and Willebrand (2001) plays a minor role on the time scales we address, these processes represent internal feedback mechanisms in our model. The second mechanism is related to the GSR overflows and the formation of NADW on the GSR slope by entrainment. Its influence on baroclinicity in the North Atlantic is smaller than the one from the internal feedback mechanisms (Fig. 19) but on the other hand it does not depend as

strongly on the SPG circulation strength as the latter. Hence it provides a certain control on the SPG system and can be regarded as an external control mechanism. However, the overflow transport is not independent from the SPG because the gyre modulates the Atlantic inflow into the Nordic Seas (Hátún et al., 2005). Based on this idea, we found an additional external feedback loop that contains the external control mechanism (Fig. 21). In our model these three feedback mechanisms allow for a bistability of the SPG.

We would like to emphasise that the presented feedback loops depend exclusively on large scale properties of the circulation. A number of small scale processes, such as eddy motion, will complicate the picture in the real ocean. In our model these are partly accounted for through a parameterisation (following Gent and McWilliams (1990)) which does not influence the phenomenon qualitatively. The representation of the overflows, which is part of the external feedback loop, is particularily coarse in our model. For the presented feedbacks, it is only necessary that the overflow waters are denser than the downwelling south of the ridge, which is the case in the model and observed in the ocean. Due to the coarse resolution of the model, deep water formation south of the Greenland-Scotland ridge is shifted from Labrador Sea towards Irminger Sea, i.e. the northwestward excursion of the SPG is not well represented in the model and the centre of the SPG is somewhat shifted to the east (around 55°N and 30°W, Fig. 13).

The stronger circulation mode in the unparameterised model version DEEP compares well with the model version with the hydraulic overflow parameterisation HYDRO (Fig. 14, 20, 23). Due to the constraints of the parametrisation the overflow/downwelling ratio is less variable and the dynamics of the external feedback mechanism are changed fundamentally. Thus HYDRO does not show multiple stable modes for the SPG and stabilises the subpolar region in the strong circulation mode. To date, a bistability of the SPG has neither been reported from ocean modelling nor exists observational evidence so that it remains questionable if a bistable SPG is realistic or, in the case it is, if a stabilising parameterisation like the one presented here suppresses an important characteristic of the oceanic variability on intermediate time scales.

A simple stability analysis with anomalous freshwater flux in the North Atlantic yielded major differences in the stability of the overflow transport, but not in that of

the AMOC in general. The parameterisation stabilises the overflows while in DEEP the overflow transport breaks down for an anomalous forcing above 0.2 Sv. With the overflow parameterisation, the Atlantic inflow is shallower and thus warmer and more saline. Consequently, the Nordic Seas freshen less in HYDRO and the deep convection in this region is more stable than in DEEP (Fig. 28). We also found a more stable AMOC if DEEP is in the strong SPG mode before application of the continuous anomalous freshwater flux (29). This indicates that the SPG influences the meridional overturning circulation. The SPG has recently been suggested to provide a certain measure for the AMOC (Häkkinen and Rhines, 2004). Our results support this, although it requires future work to identify the precise mechanisms. Measurements could easily be achieved from satellite altimetry, because the SPG strength correlates well with the local sea surface elevation (Fig. 26).

Concerning the hydraulic overflow parameterisation, the most important impact on the dynamics of the Atlantic Ocean may be the stabilisation of the strong SPG circulation mode. Complex OGCMs apply a range of other parameterisations that affect the overflow transport both in strength and density as for example bottom boundary layer models or mixing schemes (Thorpe et al., 2004). It requires further work to assess their influence on the SPG and to quantify the realistic influence of the overflows on the SPG circulation.

References

Arakawa, A. (1966). Computational design of long-term numerical integration of the equations of fuid motions. *Journal of Computational Physics*, 1:119–146.

Bacon, S. (1997). Circulation and fluxes in the north atlantic between greenland and ireland. *Journal of Physical Oceanography*, 27:1420–1435.

Bauer, E., Ganopolski, A., and Montoya, M. (2004). Simulation of the cold climate event 8200 years ago by meltwater outburst from lake agassiz. *Paleoceanography*, 19:PA3014.

Beckmann, A. and Döscher, R. (1997). A method for improved representation of dense water spreading over topography in geopotential coordinate model. *Journal of Physical Oceanography*, 27:581–591.

Blindheim, J., Borovkov, V., Hansen, B., Malmberg, S.-A., Turrell, W. R., and Østerhus, S. (2000). Upper layer cooling and freshening in the norwegian sea in relation to atmospheric forcing. *Deep-Sea Research I*, 47:655–680.

Böning, C., Scheinert, M., Dengg, J., Biastoch, A., and Funk., A. (2006). Decadal variability of subpolar gyre transport and its reverberation in the north atlantic overturning. *Geophysical Research Letters*, 33:L21S01.

Bryan, K. (1969). A numerical method for the study of the circulation of the world ocean. *Journal of Computational Physics*, 4:347–376.

Campin, J. M. and Goosse, H. (1999). Parametrization of density–driven downsloping flow for a coarse–resolution ocean model in z–coordinate. *Tellus*, 51 A:412–430.

Cane, M. A., Kamenkovich, V. M., and Krupitsky, A. (1998). On the utility and disutility of jebar. *Journal of Physical Oceanography*, 28:519–526.

Clark, P. U., Pisias, N. G., Stocker, T. F., and Weaver, A. J. (2002). The role of the thermohaline circulation in abrupt climate change. *Nature*, 415:863–869.

Clarke, R. A. (1984). Transport through the cape farewell–flemish cap section. *Rapp. P. V. Reun. Cons. Int. Explor. Mer.*, 185:120–130.

Curry, R. and Mauritzen, C. (2005). Dilution of the northern north atlantic ocean in recent decades. *Science*, 308:1772–1774.

Curry, R., McCartney, M., and Joyce, T. (1998). Oceanic transport of subpolar climate signals to mid-depth subtropical waters. *Nature*, 391:575–577.

Dickson, R. R. and Brown, J. (1994). The production of north atlantic deep water: Sources, rates, and pathways. *Journal of Geophysical Research*, 99:12,319–12,341.

Dickson, R. R., Yashayaev, I., Meincke, J., Turrell, B., Dye, S., and Holfort, J. T. (2002). Rapid freshening of the deep north altantic ocean over the past four decades. *Nature*, 416:832–837.

Eden, C. and Willebrand, J. (2001). Mechanism of interannual to decadal variability of the north atlantic circulation. *Journal of Climate*, 14:2266–2280.

Fichefet, T. and Maqueda, M. A. M. (1997). Sensitivity of a global sea ice model to the treatment of ice thermodynamics and dynamics. *Journal of Geophysical Research*, 102:12,609.

Ganachaud, A. and Wunsch, C. (2000). Improved estimates of global ocean circulation, heat transport and mixing from hydrographic data. *Nature*, 408:453–456.

Gent, P. R. and McWilliams, J. C. (1990). Isopycnal mixing in ocean circulation models. *Journal of Physical Oceanography*, 20:150–155.

Gnanadesikan, A. (1997). Representing the bottom boundary layer in the gfdl ocean model: Model framework, dynamical impacts, and parameter sensitivity. *unpublished manuscipt*.

Gölzer, H., Mignot, J., Levermann, A., and Rahmstorf, S. (2006). Tropical versus high latitude freshwater influence on the atlantic circulation. *Climate Dynamics*, 27:715–725.

Greatbatch, R. J., Fanning, A. F., Goulding, A. D., and Levitus, S. (1991). A diagnosis of interpentadal circulation changes in the north atlantic. *Journal of Geophysical Research*, 96:22,009–22,023.

Griesel, A. and Maqueda, M. A. M. (2006). The relation of meridional pressure gradients to north atlantic deep water volume transport in an ocean general circulation model. *Climate Dynamics*, 26:781–799.

Häkkinen, S. (2001). Variability in sea surface height: A qualitative measure for the meridional overturning in the north atlantic. *Journal of Geophysical Research*, 106:13,837–13,848.

Häkkinen, S. and Rhines, P. B. (2004). Decline of subpolar north atlantic circulation during the 1990s. *Science*, 304:555–559.

Hall, M. and Bryden, H. (1982). Direct estimates and mechanisms of ocean heat transport. *Deep-Sea Research*, 29:339–359.

Hansen, B. and Østerhus, S. (2000). North atlantic–nordic seas exchanges. *Progress in Oceanography*, 45:109–208.

Hansen, B., Østerhus, S., Quadfasel, D., and Turrell, W. (2004). Already the day after tomorrow? *Science*, 305:953–954.

Hasumi, H. and Suginohara, N. (1999). Effects of locally enhanced vertical diffusivity over rough bathymetry on the world ocean circulation. *Journal of Geophysical Research*, 104:23,364–23,374.

Hátún, H., Sandø, A. B., Drange, H., Hansen, B., and Valdimarsson, H. (2005). Influence of the atlantic subpolar gyre on the thermohaline circulation. *Science*, 309:1841–1844.

Hofmann, M. and Maqueda, M. A. M. (2006). Performance of a second–order moments advection scheme in an ocean general circulation model. *Journal of Geophysical Research*, 111:C05006.

Kalnay, E. and Coauthors (1996). The ncep/ncar 40-year reanalysis project. *Bull. Amer. Meteor. Soc.*, 77:437–471.

Kieke, D. and Rhein, M. (2006). Variability of the overflow water transport in the western subpolar north atlantic, 1950–97. *Journal of Physical Oceanography*, 36:435–465.

Kösters, F. (2004). Denmark strait overflow: comparing model results and hydraulic tranport estimates. *Journal of Geophysical Research*, 109:C10011.

Kösters, F., Käse, R. H., Schmittner, A., and Herrmann, P. (2005). The effect of denmark strait overflow on the atlantic meridional overturning circulation. *Geophysical Research Letters*, 32.

Kuhlbrodt, T., Griesel, A., Montoya, M., Levermann, A., Hofmann, M., and Rahmstorf, S. (2006). On the driving processes of the atlantic meridional overturning circulation. *Reviews of Geophysics*, in press.

Kunze, E., Dower, J. F., Beveridge, I., Dewey, R., and Bartlett, K. P. (2006). Observations of biologically generated turbulence in a coastal inlet. *Science*, 313:1768 – 1770.

Ledwell, J. R., Montgomery, E. T., Polzin, K. L., Laurent, L. C. S., Schmitt, R. W., and Toole, J. M. (2000). Evidence for enhanced mixing over rough topography in the abyssal ocean. *Nature*, 403:179–182.

Levermann, A., Griesel, A., Hofmann, M., Montoya, M., and Rahmstorf, S. (2005). Dynamic sea level changes following changes in the thermohaline circulation. *Climate Dynamics*, 24:347–354.

Levitus, S. (1982). *Climatological atlas of the world ocean. NOAA Professional Paper, vol 13.* US Dept of Commerce, Washington DC.

Lohmann, G. (1998). The influence of a near-bottom transport parameterization on the sensitivity of the thermohaline circulation. *Journal of Physical Oceanography*, 28:2095–2103.

Manabe, S. and Stouffer, R. J. (1988). Two stable equilibria of a coupled ocean-atmosphere model. 1:841–866.

Mertz, G. and Wright, D. G. (1992). Interpretations of the jebar term. *Journal of Physical Oceanography*, 22:301–305.

Mignot, J., Levermann, A., and Griesel, A. (2006). A decomposition of the atlantic meridional overturning circulation into physical components using its sensitivity to vertical diffusivity. *Journal of Physical Oceanography*, 36:636–650.

Montoya, M., Griesel, A., Levermann, A., Mignot, J., Hofmann, M., Ganopolski, A., and Rahmstorf, S. (2005). The earth system model of intermediate complexity clim*ber*-3α. part i: description and performance for present-day conditions. *Climate Dynamics*, 25:237–263.

Munk, W. and Wunsch, C. (1998). Abyssal recipes ii: energetics of tidal and wind mixing. *Deep-Sea Research*, 45:1977–2010.

Myers, P. G., Fanning, A. F., and Weaver, A. J. (1996). Jebar, bottom pressure torque, and gulf stream separation. *Journal of Physical Oceanography*, 26:671–683.

Østerhus, S., Turrell, W. R., Jónsson, S., and Hansen, B. (2005). Measured volume, heat, and salt fluxes from the atlantic to the arctic mediterranean. *Geophysical Research Letters*, 32:L07603.

Penduff, T., Barnier, B., and de Verdière, A. C. (2000). Self-adapting open boundaries for a sigma coordinate model of the eastern north atlantic. *Journal of Geophysical Research*, 105:11,279–11,298.

Petoukhov, V., Ganopolski, A., Brovkin, V., Claussen, M., Eliseev, A., Kubatzki, C., and Rahmstorf, S. (2000). Clim*ber*-2: a climate system model of intermediate complexity. part i: model description and performance for present climate. *Climate Dynamics*, 16:1.

Prange, M., Lohmann, G., and Paul, A. (2003). Influence of vertical mixing on the hysteresis: analysis of an ogcm. *Journal of Physical Oceanography*, 33:1707–1721.

Prather, M. J. (1986). Numerical advection by conservation of second-order moments. *Journal of Geophysical Research*, 91:6671–6681.

Rahmstorf, S. (1996). On the freshwater forcing and transport of the atlantic thermohaline circulation. *Climate Dynamics*, 12:799–811.

Rahmstorf, S. (2002). Ocean circulation and climate during the past 120,000 years. *Nature*, 419:207–214.

Rahmstorf, S., Crucifix, M., Ganopolski, A., Goosse, H., Kamenkovich, I., Knutti, R., Lohmann, G., Marsh, B., Mysak, L. A., Wang, Z., and Weaver, A. (2005).

Thermohaline circulation hysteresis: a model intercomparison. *Geophysical Research Letters*, 32:L23605.

Read, J. (2001). Water masses and circulation of the northeast atlantic subpolar gyre. *Progress in Oceanography*, 48:461–510.

Redler, R. and Böning, C. W. (1997). Effect of the overflows on the circulation in the subpolar nort atlantic: A regional model study. *Journal of Geophysical Research*, 102:18,529–18,552.

Roberts, M. J. and Wood, R. A. (1997). Topographic sensitivity studies with a bryan cox–type ocean model. *Journal of Physical Oceanography*, 27:823–836.

Sarkisyan, A. S. and Ivanov, V. F. (1971). Joint effect of baroclinicity and bottom relief as an important factor in the dynamics of sea currents. *Izvestiya Akademii Nauk SSSR Fizika Atmosfery i Okeana*, 7(2):173–188.

Schmittner, A. (2005). Decline of the marine ecosystem caused by a reduction in the atlantic overturning circulation. *Nature*, 434:628–633.

Schmittner, A. and Weaver, A. (2001). Dependence of multiple climate states on ocean mixing parameters. *Geophysical Research Letters*, 28:1027–1030.

Stommel, H. (1961). Thermohaline convection with two stable regimes of flow. *Tellus*, 13:224–230.

Thorpe, R. B., Wood, R. A., and Mitchell, J. F. B. (2004). Sensitivity of the modelled thermohaline circulation to the parameterisation of mixing across the Greenland-Scotland ridge. *Ocean Modelling*, 7:259–268.

Timmermann, A., An, S. I., Krebs, U., and Goosse, H. (2005). Enso suppression due to weakening of the north atlantic thermohaline circulation. *Journal of Climate*, 18:2842–2859.

Toggweiler, J. R. and Samuels, B. (1993). New radiocarbon constraints on the upwelling of abyssal water to the ocean's surface. *The Global Carbon Cycle*, pages 303–331.

Toggweiler, J. R. and Samuels, B. (1995). Effect of drake passage on the global thermohaline circulation. *Deep-Sea Research*, 42:477–500.

Toggweiler, J. R. and Samuels, B. (1998). On the ocean's large scale circulation in the limit on no vertical mixing. *Journal of Physical Oceanography*, 28:1832–1852.

Treguier, A. M., Theetten, S., Chassignet, E. P., Penduff, T., Smith, R., Talley, L., Beismann, J. O., and Böning, C. (2005). The north atlantic subpolar gyre in four high–resolution models. *Journal of Physical Oceanography*, 35:757–774.

Trenberth, K. E. and Caron, J. M. (2001). Estimates of meridional armosphere and ocean heat transport. *Journal of Climate*, 14:3433–3443.

Vellinga, M. and Wood, R. A. (2002). Global climatic impacts of a collapse of the atlantic thermohaline circulation. *Climatic Change*, 54:251–267.

Whitehead, J. A., Leetma, A., and Knox, R. A. (1974). Rotating hydraulics of strait and sill flows. *Geophysical Fluid Dynamics*, 6:101–125.

List of Figures

List of Tables

A Barotropic streamfunction and explicit free surface

The definition of a streamfunction includes that its isolines must always be parallel to the stream lines of the fluid. In other words:

$$\mathbf{U} \cdot \nabla \psi = \mathbf{0}, \tag{12}$$

with $\mathbf{U} = (U, V)$. We can simplify the problem to two dimensions because the streamfunction describes the vertically integrated transport. U and V represent the vertically integrated velocities. In order to meet 12, it is sufficient to assume that $\nabla \cdot \psi = (V, -U)$, which then yields the continuity equation:

$$\begin{aligned} \partial_y \partial_x \psi + \partial_x \partial_y \psi &= 0 \\ \partial_x \psi = V, \quad \partial_y \psi &= -U \\ \partial_y V &= -\partial_x U. \end{aligned} \tag{13}$$

the two–dimensional continuity equation $\nabla \mathbf{U} = \mathbf{0}$ (equation (13)) is no longer valid with explicit free surface because of wave motion $\partial_t \eta$ and freshwater exchange with the atmosphere through precipitation and evaporation, q, that create sources and sinks of volume:

$$\nabla \cdot \mathbf{U} = -\partial_{\mathbf{t}} \eta + \mathbf{q}. \tag{14}$$

Concerning equilibrium states the temporal variations in the sea surface height could be neglected, but due to the open–boundary transport q volume conservation can not be fullfilled.

B Comments of the hydraulic transport integral

Kösters et al. (2005) refer to the overflow transport (equation (1)) as the integral form of the following equation by Whitehead et al. (1974) and argue it yields the same result when applied on a 2–layer ocean:

$$Q_{WLK} = \frac{1}{2} g' H^2, \qquad g' = \frac{\Delta\rho}{\rho_0} g, \tag{15}$$

where g' is the so–called reduced gravity. We apply equation (1) on a 2–layer ocean as depicted in figure 6 with the horizontal interface height i defined by the transition layer between ρ_1 and ρ_2 (Fig. 6).

$$Q = \frac{g}{f\,\rho_0} \left\{ \int_h^i dz\, (\rho_N - \rho_S)\, z + \int_i^\eta dz\, (\rho_N - \rho_S)\, z \right\} \tag{16}$$

The second term vanishes because above i the difference $(\rho_N - \rho_S)$ is zero above i. Densities ρ_N and ρ_S are depth–independent now and equation (16) integrates to

$$Q = \frac{1}{2} \frac{\Delta\rho_h}{\rho_0} g H^2 \tag{17}$$

Kösters et al. (2005) accept the term $\frac{\Delta\rho_h}{\rho_0}$ as the reduced gravity g', while originally it should contain the vertical density difference rather than the horizontal one. The argument that equation (1) is equivalent to equation (15) is correct for a 2–layer ocean because here the two density differences are equal, but for a three–dimensional model it is not. We do not want to overestimate this disagreement as it may be accounted for an acceptable error when applying a simplified model and other assumptions may overrule it. Yet, the parameterisation looses parts of its physical justification.

C Comparison of the parameterised model version HYDRO with the Climatology

Although the experiment hydraulic overflow parameterisation (HYDRO) shows a more realistic tracer distribution in the Nordic Seas than the unparameterised model version with artificially deepened passages (DEEP), the temperature is still too high, especially at depth. A comprehensive discussion of the shortcomings of the model can be found in Montoya et al. (2005). In addition to this figure 32 shows the differences of HYDRO to the climatology by Levitus (1982).

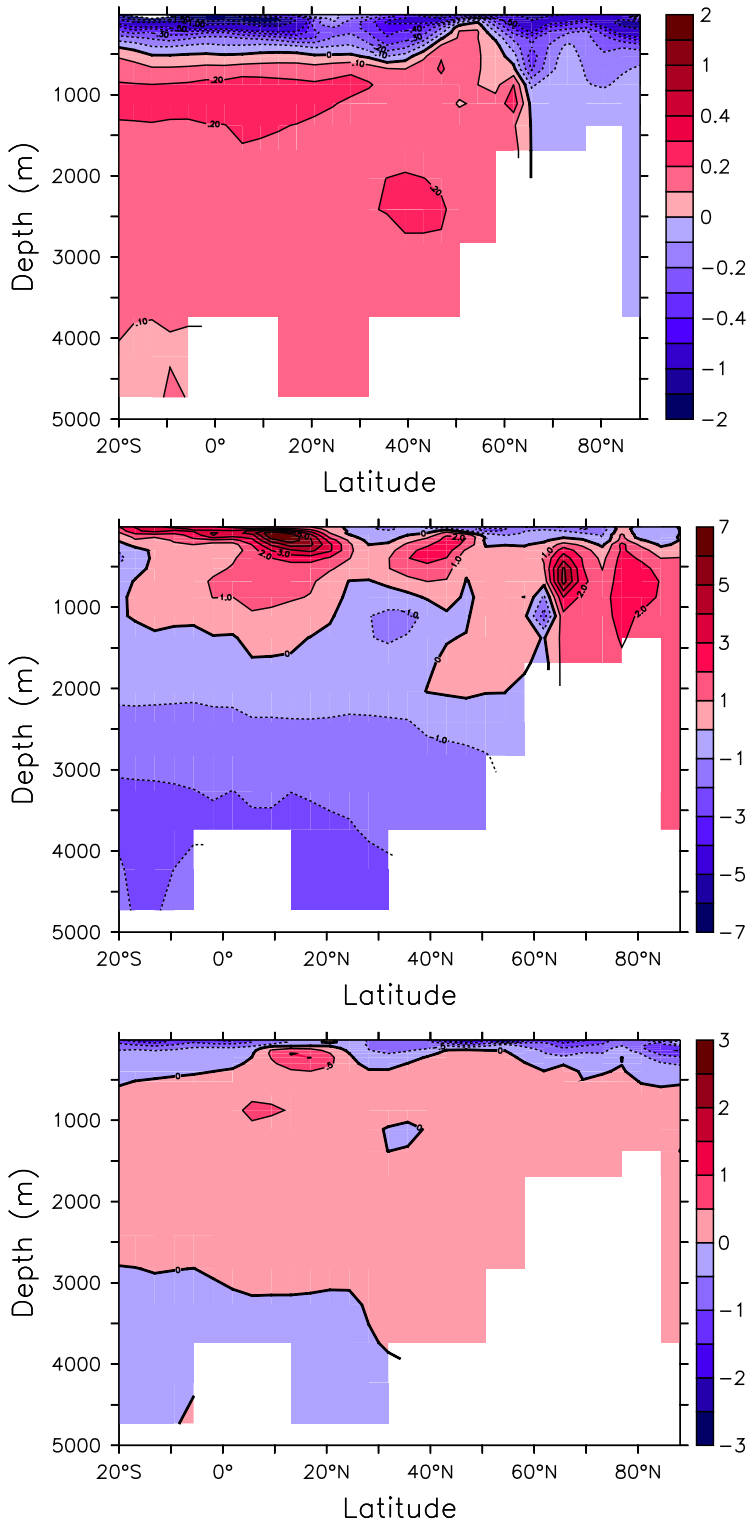

Figure 32: Differences in the tracer distribution of the parameterised model version HYDRO to the Levitus (1982) climatology (HYDRO - LEVITUS). Upper: potential density ($\frac{kg}{m^3}$), middle: temperature (K), lower: salinity (psu). The sections have been averaged zonally from 50°W to 30°E excluding the Mediterranean.

Danksagung

An dieser Stelle möchte ich mich herzlich bei allen bedanken, die mir diese Arbeit ermöglicht und mich bei ihrer Durchführung unterstützt haben. Besonders die intensive Betreuung durch Prof. Dr. Anders Levermann war mir eine große Motivation. Seine aktive Hilfe umfasste alle Bereiche dieser Arbeit. Darüber hinaus hat er mir eine effektive Arbeitsweise und nicht zuletzt Spaß an der Arbeit und der Wissenschaft vermittelt. Wichtige Unterstützung habe ich auch durch Dr. Juliette Mignot erhalten. Zuerst durch eine umfangreiche Einführung in die technischen Details der Klimamodellierung und später durch hilfreiche Kommentare zum Verfassen wissenschaftlicher Texte. Mein Dank gilt auch Dr. Matthias Hofmann, ohne dessen Vorbereitung diese Arbeit nicht hätte realisiert werden können. Später stellte er mir bereitwillig weiteren Programmcode zur Verfügung, der diese Arbeit bereichert hat. Für die Einladung an das Potsdam Institut für Klimafolgenforschung bedanke ich bei Prof. Dr. Stefan Rahmstorf wie auch für die sehr gute Ausstattung meines Arbeitsplatzes. Von nicht zu unterschätzendem Wert waren sicherlich auch die Diskussionen mit ihm im 'ocean group meeting', auch diejenigen an denen ich nur als Zuhörer teilgenommen habe. Schließlich habe ich von vielen Mitgliedern der Arbeitsgruppe Unterstützung erfahren. Nicht vergessen möchte ich an dieser Stelle Heiko Gölzer, der mir mehrfach technische Fragen beantwortete und Lösungen aufzeigte und Maik Stöckmann, dessen Gesellschaft meinen Büroalltag positiv geprägt hat.

Bedanken möchte ich mich auch bei meiner Familie, die mich ich vielerlei Hinsicht unterstützt hat, auch finanziell. Unnötig zu sagen, dass ich auch ohne ihre Hilfe diese Arbeit nicht hätte anfertigen können. Unmittelbare Hilfe leistete mir Cristina Díaz Gandía bei der Fehlerkorrektur in letzter Sekunde.

Ich erkläre hiermit, dass ich die vorliegende Arbeit selbständig verfasst und keine anderen als die angegebenen Quellen und Hilfsmittel verwendet habe.

Potsdam, den 21. Dezember 2006

Andreas Born